

# Investigation of Capstan Friction and its Potential Use as a Mechanical Amplifier

A thesis presented to

the faculty of

the Russ College of Engineering and Technology of Ohio University

In partial fulfillment

of the requirements for the degree

Master of Science

Michael M. Starkey

June 2010

© 2010 Michael M. Starkey. All Rights Reserved.

This thesis titled  
Investigation of Capstan Friction and its Potential Use as a Mechanical Amplifier

by  
MICHAEL M. STARKEY

has been approved for  
the Department of Chemical and Biomolecular Engineering  
and the Russ College of Engineering and Technology by

---

Robert L. Williams II  
Professor of Mechanical Engineering

---

Dennis Irwin  
Dean, Russ College of Engineering and Technology

## ABSTRACT

STARKEY, MICHAEL M., M.S., June 2010, Biomedical Engineering

Investigation of Capstan Friction and its Potential Use as a Mechanical Amplifier

(103 pp.)

Director of Thesis: Robert L. Williams II

Actuation is one of the fundamental aspects of robots. Optimization of a robotic system poses a complex problem for engineers. For developing robots that mimic biological systems, the robot actuation problem becomes more complicated because of stringent limitations on space and power output.

It is hypothesized that a system can be designed which would allow a rotating capstan to act as a mechanical amplifier when a flexible member such as a cord or rope is wrapped around it. When a tension is applied to the end of the cord pointing in the direction of the capstan's rotation, friction will be transferred to the cord and the tension will effectively be amplified.

Experimentation was performed to validate a traditional assumption for how the dynamics of the system should work. The capstan equation was found to be only a rough estimation of the behavior of the system. A new equation was formed by combining known curves and fitting them to the data. Simulation of the new equation provides an initial insight into the behavior of a combined capstan amplifier system.

Approved: \_\_\_\_\_

Robert L. Williams II

Professor of Mechanical Engineering

## ACKNOWLEDGMENTS

I would like to take the time to sincerely thank the many people who helped me achieve all of which I have been able to. To my parents I would like to thank them for all of the hard work they have put in to allow me to rise to the level to which I have. Also, I would like to thank my family in general for always being there with support and encouragement. For academic guidance I would like to thank Dr. Robert Williams for supporting me throughout college and encouraging me to constantly pursue new heights. My thesis board has provided me with incredible guidance and constructive criticism which has allowed this document to become a work in which I am very proud of. Finally I would like to acknowledge Dr. Choi for lending me the equipment necessary to complete the testing.

## TABLE OF CONTENTS

	Page
Abstract.....	3
Acknowledgments.....	4
List of Tables .....	8
List of Figures.....	9
List of Terms.....	13
Background.....	14
Literature Review .....	18
Existing Systems.....	18
Unidrive Robotics .....	20
Capstan Friction .....	21
Project Background.....	22
Motivation.....	22
Underlying Theory.....	24
Thesis Objectives .....	27
Experimental Setup.....	28
Device .....	28
Control .....	30
Circuitry .....	30
Program.....	31
Procedure .....	32

	6
Results.....	35
Diameter Consideration .....	36
Angular Velocity Consideration .....	39
Belt Friction Adherence .....	42
Theory on Fast Rising Region .....	67
Simulation.....	69
Discussion.....	73
Conslusions and recommendations.....	75
Conclusions.....	75
Recommendations.....	76
Testing of Multiple Control Motors.....	76
Capstan and Cord Materials.....	76
Full System Integration.....	77
References.....	78
Appendix.....	80
Arduino Code.....	81
Comparison between Data and Estimation Equation .....	83
MATLAB Code .....	85
Experimental Simulation .....	85
Two Control, Single Drive System.....	88
Simulink Models.....	90
Conditioned Data .....	93

0.5 Inch capstan ..... 94

1.0 Inch capstan ..... 99

## LIST OF TABLES

	Page
Table 1 - Friction values for exponential fit .....	42
Table 2 - Exponential decay variables used for curve fitting .....	51
Table 3 - Double exponential full curve variables.....	57

## LIST OF FIGURES

	Page
Figure 1 - Railing mounted capstan .....	16
Figure 2 - Cassette Tape Capstan.....	16
Figure 3 - Theoretical System.....	17
Figure 4 - Uni-drive schematic (Karbasi, Huissoon and Khajepour 2004) .....	20
Figure 5 - Uni-drive clutch (Karbasi, Huissoon and Khajepour 2004).....	21
Figure 6 - FBD of capstan derivation (Attaway 1999) .....	25
Figure 7 - Experimental Setup .....	29
Figure 8 - Close up view of servo platform .....	30
Figure 9 - Circuit diagram.....	31
Figure 10 - T2 vs T1 - 0.5" Diameter .....	35
Figure 11 - T2 vs T1 - 1.0" Diameter .....	36
Figure 12 - 270 Degree run comparison .....	37
Figure 13 - 360 Degree run comparison .....	37
Figure 14 - 450 Degree run comparison .....	38
Figure 15 - 630 Degree run comparison .....	38
Figure 16 - 720 Degree run comparison .....	39
Figure 17 - 360 Degree rotational speed comparison .....	40
Figure 18 - 450 Degree rotational speed comparison .....	40
Figure 19 - 630 Degree rotational speed comparison .....	41
Figure 20 - 720 Degree rotational speed comparison .....	41

Figure 21 - T2 vs T1 - 0.5" Diameter with capstan equation curve fit .....	43
Figure 22 - T2 vs T1 - 1.0" Diameter with capstan equation curve fit .....	43
Figure 23 - Plot of Amplification (T2/T1) - 0.5" Diameter .....	44
Figure 24 - Plot of Amplification (T2/T1) - 1.0" Diameter .....	45
Figure 25 - Theoretical amplification curves for capstan equation – 0.5" Diameter .....	46
Figure 26 - Theoretical amplification curves for capstan equation - 1.0" Diameter .....	46
Figure 27 - Amplification comparison at 270 degrees.....	47
Figure 28 - Amplification comparison at 360 degrees.....	48
Figure 29 - Amplification comparison at 450 degrees.....	48
Figure 30 - Amplification comparison at 630 degrees.....	49
Figure 31 - Amplification comparison at 720 degrees.....	49
Figure 32 - 270 degree - amplification fit - exponential decay.....	51
Figure 33 - 360 degree - amplification fit - exponential decay.....	52
Figure 34 - 450 degree - amplification fit - exponential decay.....	52
Figure 35 - 630 degree - amplification fit - exponential decay.....	53
Figure 36 - 720 degree - amplification fit - exponential decay.....	53
Figure 37 - Comparison between angle of contact and SS term of the exponential .....	54
Figure 38 - Comparison between angle of contact and No term of the exponential .....	55
Figure 39 - Slow decrement region plot comparison between angles of contact .....	56
Figure 40 - Double exponential full curve fit - 270 degrees.....	58
Figure 41 - Double exponential full curve fit - 360 degrees.....	58
Figure 42 - Double exponential full curve fit - 450 degrees.....	59

	11
Figure 43 - Double exponential full curve fit - 630 degrees.....	59
Figure 44 - Double exponential full curve fit - 720 degrees.....	60
Figure 45 - Relationship between Nd term of the double exponential and the angle of contact.....	62
Figure 46 - Relationship between the Lambda d term of the double exponential and the angle of contact.....	62
Figure 47 – Theoretical curves describing the experimental plots of amplification.....	63
Figure 48 - Performance of double exponential fit to the experimental data - 270 degrees.....	64
Figure 49 - Performance of double exponential fit to the experimental data - 360 degrees.....	65
Figure 50 - Performance of double exponential fit to the experimental data - 450 degrees.....	65
Figure 51 - Performance of double exponential fit to the experimental data - 630 degrees.....	66
Figure 52 - Performance of double exponential fit to the experimental data - 720 degrees.....	66
Figure 53 - Double exponential estimation curves for experimental data.....	67
Figure 54 - Possible cord deformation causing fast rising region in data.....	68
Figure 55 - Simulated experimental data comparing T2 to T1.....	69
Figure 56 - Simulated amplification (T2/T1) for the test data.....	70
Figure 57 - Sample test input for control motor 1 in simulation .....	71

	12
Figure 58 - Periodic stepping input provided by control motor 2 in simulation .....	71
Figure 59 - Simulated estimate for the drive current needed for amplification.....	72
Figure 60 – Simulated estimate of drive motor power consumption.....	72
Figure 61 - Comparison between the experimental data and the double exponential estimation equation – 0.5” Diameter .....	83
Figure 62 - Comparison between the experimental data and the double exponential estimation equation – 1.0” Diameter .....	84
Figure 63 - Full system Simulink model.....	90
Figure 64 - Servo Simulink subsystem .....	90
Figure 65 - Capstan Simulink subsystem .....	91
Figure 66 - Simulink subsystem to calculate $\Lambda d$ .....	91
Figure 67 - Simulink subsystem to calculate $N_o$ .....	91
Figure 68 - Simulink subsystem to calculate steady state (SS) .....	91
Figure 69 - Simulink subsystem to calculate $N_d$ .....	92
Figure 70 - Two control, single drive system simulation .....	92

## LIST OF TERMS

T1	Smaller tension in the capstan equation
T2	Greater tension in the capstan equation as a result of the mechanical amplification
$\mu$	Coefficient of friction used in the capstan equation
$\beta$	Angle in radians in which the flexible member is in contact with the capstan
No	The magnitude of the slow decay region exponential used in the double exponential
$\lambda$	The rate of decay term used to describe the slow decay region in the double exponential
Nd	The magnitude of the fast rising region exponential used in the double exponential equation
$\lambda_d$	The rate of decay term used to describe the fast rising region in the double exponential
SS	The value at which the double exponential equation reaches when the transient fast rising region and slow decay region have died out.

## Chapter 1: introduction

### Background

Since the inception of robotics, humans have been trying to mimic the design of biological systems. Attempt after attempt brings new innovations and moves technology closer to being able to fully mimic a biological system. The path to this realization has numerous roadblocks imparted by the complexity of biological systems. Almost every aspect about recreating a biological system poses a difficult engineering problem. The main engineering hurdle in creating biomimetic robots, as far as actuation is concerned, is to maximize the force output while reducing the power input. This problem is common in engineering but presents an especially challenging one for biomimetics.

Biological systems have been evolving for billions of years. Natural selection has led to many biomechanical adaptations to movement involving the use of biological energy. Ants are able to lift numerous times their own body weight, cheetahs can reach speeds in excess of sixty miles an hour and humans can perform tasks too complicated for current robotics to recreate. Evolutionary innovations have allowed these systems to perform as well as they do but in the same light, make it hard for other systems such as robotics to mimic them. The source of motion in biological systems is commonly muscle. It can generate high forces and contract at high velocity; all while using relatively low amounts of energy. To be able to mimic these traits would allow biomimetic robotics to behave and appear closer to the biological systems.

Every innovation comes with additional limitations. Historically the method for animating robots is through the use of geared directly driven linkages. This method

provides high torques, high velocities and high levels of precision. Electric motors however need many windings to develop high torque which lead to increased weight and heat production. Other methods of biomimetic actuation include pneumatics, hydraulics and electrically reactive alloys. For pneumatics and hydraulics, the systems are able to generate the needed forces but suffer from the inclusion of valves, fluid (hydraulics) and the pump/motor assembly; each adds weight and takes up valuable space. There have been numerous designs for biomimetic robotics which use these methods. However, they are further burdened by the fact that driving pressures come from sources external to the moving system. The electrically reactive alloys are newer in concept but the limitations include high power consumption, low force generation and low actuation speed. Their size, however, makes them attractive for smaller robotics where high forces may not be necessary and space is at a high premium.

The scope of this project is with larger biomimetic robotics on a scale comparable to humans. The needs of this scale include high forces, minimal weight and volume, low power consumption and in some applications the ability to rapidly apply the forces. The system which will be studied aims to provide a more efficient drive scheme to be used in biomimetic robotics

The underlying principle behind the system is capstan friction or belt friction. Belt friction involves the friction developed when a deformable body such as a cable or belt is wrapped around a rigid body such as a rod. Capstans are common place on ships (Figure 1) and can also be found tape format electronics (Figure 2), although with a slightly different application. Boats, especially ones with larger sails, include a device

usually affixed to the railings which is called a capstan winch. A capstan winch is a polished concaved cylinder driven by a geared motor. When a rope is wrapped around the capstan, a deck hand is able to pull on the loose end of the rope and develop friction between the rope and the capstan (Figure 1).

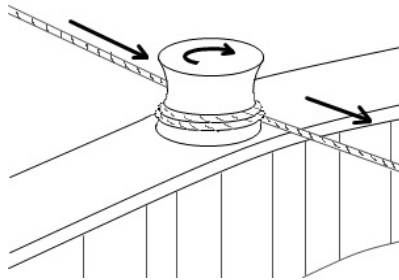


Figure 1 - Railing mounted capstan

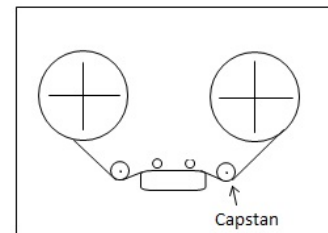


Figure 2 - Cassette Tape Capstan

The friction developed in this process is able to transfer most of the needed force to the capstan driver rather than the human, allowing for heavier things to be hoisted. This concept of force transference is the underlying principle in this investigation. The goal of this study is to test the hypothesis that small scale capstan-based mechanical amplifiers might be feasible for application in human scale robotic motion. By using the capstan theory, a system could be developed which utilizes a single large drive motor acting as the mechanical amplifier and numerous smaller control motors controlling the motion and force in a cable. An illustrated example of what the system could resemble is shown in Figure 3. In Figure 3, there is a single large drive motor with four smaller motors surrounding it. There are four cords, each attached to a separate small motor. Each of the cords is wrapped around the drive motors capstan. The drive motor would then be able to act as an amplifier for each of the individual small motor setups.

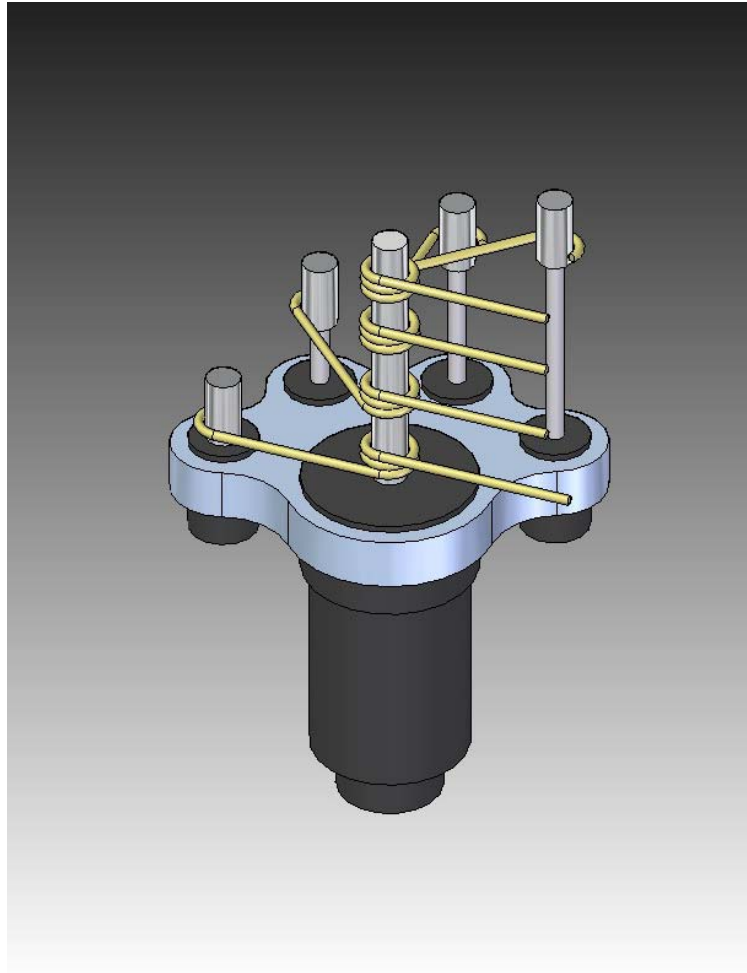


Figure 3 - Theoretical System

## Literature Review

### *Existing Systems*

The idea of biomimetic robots has been around since the birth of robotics. Biological systems provide a challenge for engineers both from their complexity and from their size. Modeling of biological systems ranges from the basic oscillatory motion of a swimming fish to the infinite degree of freedom continuum robots which mimic the trunk of an elephant or leg of an octopus (Camarillo, Carlson and Salisbury, Configuration Tracking for Continuum Manipulators With Coupled Tendon Drive 2009) (Camarillo, Milne, et al. 2008). Perhaps easier and more intuitive to understand are the biomimetic robots which mimic the anatomy of vertebrates.

All vertebrates create motion via muscles that control the movements of skeletal elements. Numerous biomimetic robots employ directly driven linkages in attempt to simplify the control and mathematics, however the more accurate robots simulate the actual anatomical joints with cable actuated links. The greatest challenge to these biomimetic robots is providing the necessary power within the space and mass limits of vertebrate joint systems. A common practice is to tether the robot and power it remotely. This is usually done when the focus of a project is on the kinetics and control rather than mobility (Koo, et al. 2009) or in an application which allows for it such as (Kong and Jeon 2006). True biomimetic robots often lack the luxury of continuous power supply of stationary robots. In addition to limited power supply, they also have to cope with limited weight and space. The need to carry both the batteries and the driving actuators adds large amounts of weight which results in more power needed to control them. This

concept is clearly illustrated by the humanoid robot developed by Honda. The robot was completely untethered, but only had a battery life of 15 minutes and the batteries weighing 20 kg (Hirai, Hirose and Takenaka 1998).

To overcome some of the weight issues and make the robot more efficient, a common practice is to under actuate the movements (Ghorbani and Wu 2009). Under actuation is produced by using fewer motors than there are degrees of freedom. The remaining degrees of freedom are actuated through passive means usually with the inclusion of springs (Iida, Rummel and Seyfarth 2008). The obvious short coming of utilizing under actuated robots is the sacrificing of control. For many applications of robotics this may be an appropriate simplification but when full control is needed the challenge becomes how to actuate the system with the allowable weight and power.

A classic example of the struggle between control and weight is the development of a biomimetic hand. There have been numerous studies and biomimetic hands developed (Lin and Huang 1998) (Jones 1997). The human hand poses a great challenge to engineering design. With relatively small volume and “over 20 degrees of freedom” (Bundhoo and Park 2005), it becomes very difficult to achieve similar motion with electric motors. Researchers have tried numerous arrangements for the motors even to the point of integrating micro motors with huge gearing ratios into the fingers of their robotic hands (Lin and Huang 1998). The problems still come down to providing large amounts of force with as little space as possible

### Unidrive Robotics

Unidrive robots are a class of robots which are defined by “one drive motor mounted at the base [which] is used to power all modules through a rotating shaft and clutches” (Karbasi, Huissoon and Khajepour 2004). The clutches in the system act similarly to the clutch in an automobile. When the clutch is engaged, power is taken from the drive shaft and used to actuate some other part of the system. This system is shown in Figure 4 below. There are two configurations shown in Figure 4; a serial and a parallel.

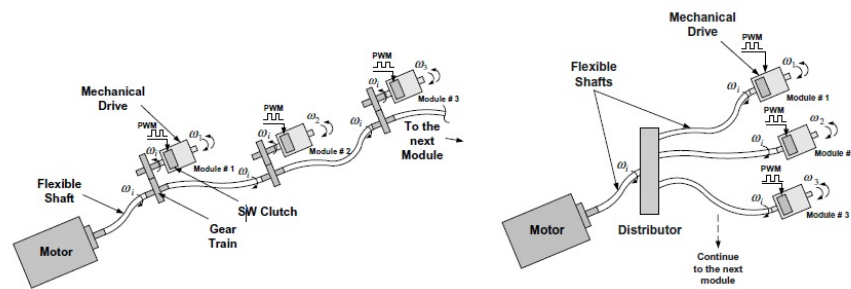


Figure 4 - Uni-drive schematic (Karbasi, Huissoon and Khajepour 2004)

This single source of the power in the uni-drive setup is a beneficial application of capstan friction. Having the main large motor allows for the weight to be localized allowing for greater mechanical efficiency when actuating serial linkages. This study looks to replicate the clutch control system with a capstan based actuation scheme. Using the clutch system has one important disadvantage; the size of the clutches. Figure 5 shows one of the clutches used in the system. There is a pencil in the photo for size comparison. The scope of the project for which this clutch was developed was a linear

positioning table so the size wasn't an issue, but for mobile biomimetic robots useful scalability of the clutch system becomes a critical issue.

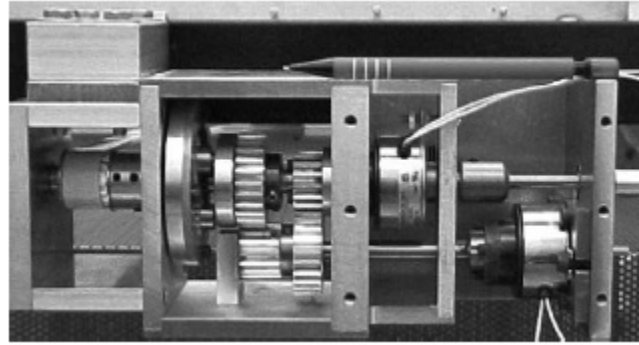


Figure 5 - Uni-drive clutch (Karbasi, Huissoon and Khajepour 2004)

Another disadvantage present in uni-drive systems is the mechanical crosstalk inherent in the system. The drive motor is actuating all of the subsystems therefore any disturbance in a subsystem will be felt by the drive motor and back down to all of the other subsystems (Li, Liu and Ming 2008). This issue will also need to be studied in a capstan implementation.

In addition to the crosstalk, uni-drive systems have to pull power from the shaft. Whether by clutch or some other means, there will be a degree of error associated with the method of engagement. In Karbasi and Khajepour (2004) this error came from the periodic PWM engaging of the clutch which introduced consistent error into the system.

#### *Capstan Friction*

The key factor for the capstan amplifier to work is its ability to develop friction between the cables and drive shaft. The friction is model which is used to determine the developed friction is the capstan friction equation shown as Equation 1 (Attaway 1999).

$$T_2 = T_1 e^{\mu\beta} \quad (1)$$

The equation describes a ratio between the input tension  $T_1$  and the output tension  $T_2$ . The friction coefficient is defined as  $\mu$  and the  $\beta$  term is the angle in radians in which the cable is in contact with the drive shaft. The exponential serves as the amplification factor which the drive system utilizes. Nonlinearity in the friction equation has been described in textile applications suggesting the conventional equation may not hold (Jung, Pan and Kang 2008) (Tu and Fort 2004) and may have use for the drive system depending on cable make up, but for the preliminary modeling the simple capstan friction equation will be used.

## Project Background

### *Motivation*

The focus of this project is a proof of concept. The concept being studied is the capstan force assist. Similarly to how the capstan assists a crew member in lifting loads well out of physical limitations, the same principle should be able to be applied to robotics. In the place of the crew member would be a small control motor which would control the tension developed in the cable. The cable would then be wrapped around a capstan driven by a larger motor as illustrated in Figure 3.

After being wrapped around the driving capstan, the cable would then attach to the linkage or body being actuated. In this setup, because of belt friction, the driving capstan will act as a mechanical amplifier. As a result of adding the drive motor, the control motor can be greatly reduced in size because it will have to output less force.

Intuitively the drive scheme might not make sense since a linkage could be directly driven simply by a geared motor so the new system would add unnecessary complexity. It would also seem that the system will use more power driving two motors and that both motors would add additional weight. For a single control motor and drive motor this would most likely be the case. The hypothesized benefit would come from the addition of numerous control motors.

Biological systems, with respect to locomotion, usually actuate themselves with muscle attached to tendons. This system is analogous to cable tendon robots. To have full control of a linkage in a tendon robot, two motors must be incorporated to actuate the antagonist tendons (cables). For a single link, this doubles the weight associated with the driving motors. For a fixed robot this may only be an inconvenience but for mobile robots the added weight may be unacceptable for most applications. Under actuation is an option where, with the help of springs and other means, motors can be replaced and the function partially conserved.

The capstan drive scheme aims to replace the two large actuating motors with a single large driving motor and two smaller control motors (a simpler version of the theoretical setup shown in Figure 3). Again this might seem like there is added complexity, but with the addition of the second control motor the benefits begin to become apparent. For the tendon robot system with two large motors, because of the antagonist nature of the actuation, only one motor is generating force at any given time (stabilization can be accomplished by the antagonist motor but it will be with relatively

minimal force). This means that the second motor is acting as dead weight while not in use.

The new drive scheme should help to eliminate this unnecessary weight. Since the drive motor acts to amplify the output force developed by the control motors, the two small control motors act as the two large driving motors in the standard system. The benefit however is that the weight of the two control motors and the large drive motor is much less than the standard two motor design. Adding additional control motors to the system would only increase the weight efficiency while possibly increasing overall efficiency due to reduced control electronics and power requirements. This is the concept that will either be proven or disproven to work. The first step in the investigation involves preliminary mathematical simulation which will be shown in the accomplished work section. Additional mathematical simulation will be used to determine the logistics of operating multiple control motors off the same drive motor. When the simulations have been completed, a physical model will be constructed to test if the system operates in the real world.

#### *Underlying Theory*

The theory which is being tested is the capstan equation theory which is hypothesized to describe the friction characteristics of a flexible member such as a cord or belt wrapped around a cylinder. The free body diagram for the derivation of the capstan friction equation is shown in Figure 6.

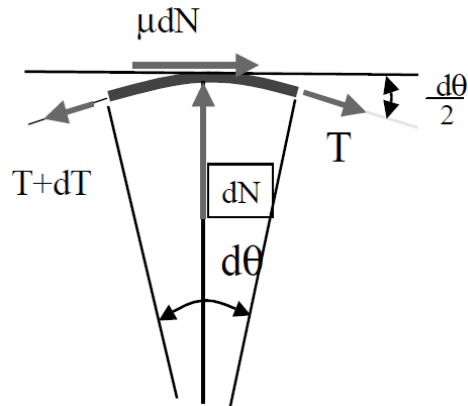


Figure 6 - FBD of capstan derivation (Attaway 1999)

The forces are first summed in the x (horizontal) direction

$$T \cos \frac{d\theta}{2} + \mu dN = (T + dT) \cos \frac{d\theta}{2} \quad (2)$$

This equation effectively reduces down to

$$\mu dN = dT \quad (3)$$

The forces similarly summed in the y (vertical) direction yielding

$$dN = (T + dT) \sin \frac{d\theta}{2} + T \sin \frac{d\theta}{2} \quad (4)$$

Similar to the summation in the x direction, Equation 4 can be reduced to

$$dN = T d\theta \quad (5)$$

Combine Equations 3 and 5

$$\frac{dT}{T} = \mu d\theta \quad (6)$$

Integrate over the range of tensions and the angle of contact,  $\beta$

$$\int_{T_1}^{T_2} \frac{dT}{T} = \int_0^{\beta} \mu d\theta \quad (7)$$

Solve

$$\ln \frac{T_2}{T_1} = \mu\beta \quad (8)$$

Simplify to the capstan friction equation

$$T_2 = T_1 e^{\mu\beta} \quad (9)$$

It can be noted that the capstan equation does not take into consideration the radius or total area of contact the flexible member has with the cylinder.

## THESIS OBJECTIVES

To verify the feasibility of the hypothesized system, specific steps must be taken. The function of the system relies on the capstan equation to hold true. Before an simulation or construction can take place the validity of this equation must be tested. Only after this has been done can any simulation be accurately constructed. If the capstan equation is unable to describe the behavior of the system, a new equation or set of equations must be formulated and described.

Upon deriving a suitable equation for describing the characteristics of the capstan friction, a simulation can be constructed which would both verify the test data and allow for insight into possible applications for the system. After simulation, a physical system may be constructed to test the real world functionality.

The objectives of this thesis are enumerated as follows:

1. Compare the behavior of an experimental capstan to the theoretical behavior dictated by the belt friction equation.
2. Integrate the findings from Objective 1 into the mathematical simulation.
3. Construct a mechanical amplifier using a single rotating capstan with a single control motor and observe the operational behavior with respect to Objective 1.
4. Compare the results from Objective 3 with the theoretical behavior predicted by the simulation and make changes to the simulation if found to be incongruent.
5. Construct a system similar to Figure 3 which utilizes a single drive motor with additional control motors producing tension. Characteristics such as friction and crosstalk will be observed.
6. Compare the system performance to other methods of actuation with respect to weight, output and power consumption.

## Testing

In the following sections, both the experimental setup for the testing apparatus and the results are presented.

### Experimental Setup

#### *Device*

To explore the belt friction phenomena, a testing setup had to be designed so that the different aspects which may contribute to the functionality of the system may be isolated. A simple system consisting of a single rotating capstan with a single flexible member wrapped about it was chosen for this reason. The testing system was oriented horizontally to eliminate the effects of gravity.

The testing device was constructed out of HDPE 10" disks. There are three disks separated with nuts allowing the ability to change the spacing between them. The circular design allows for the force sensors to be rotated and locked down at differing angles. The drive motor is affixed to the underside of the top disk and protrudes its shaft up through the disk to allow for variable sized capstans to be attached. The testing structure is shown with the white disks in Figure 7. There is a movable platform with an attached servo motor which is used to develop the tension in the cord. A closer view of the servo platform is shown in Figure 8.

Data acquisition is accomplished by a LabPro data logger connected via USB to a PC running Logger Pro 3.6. Power is supplied to the drive motor via a Vernier Power

Amplifier. An Arduino microcontroller supplies the control voltage to both the power amplifier and to the servo motor.



Figure 7 - Experimental Setup



Figure 8 - Close up view of servo platform

### *Control*

The Arduino microcontroller is programmed with the specific procedure to carry out. When a control button is depressed which is attached to the Arduino, the program commences. Within the program a trigger signal is sent to the LabPro which in turns begins the data acquisition. As the program proceeds, the servo motor increases its angle in a step wise manner. This displacement causes tension to be developed in the string.

### *Circuitry*

The wiring diagram for the Arduino board is shown in Figure 9. The Arduino microcontroller is supplied with 9V DC.

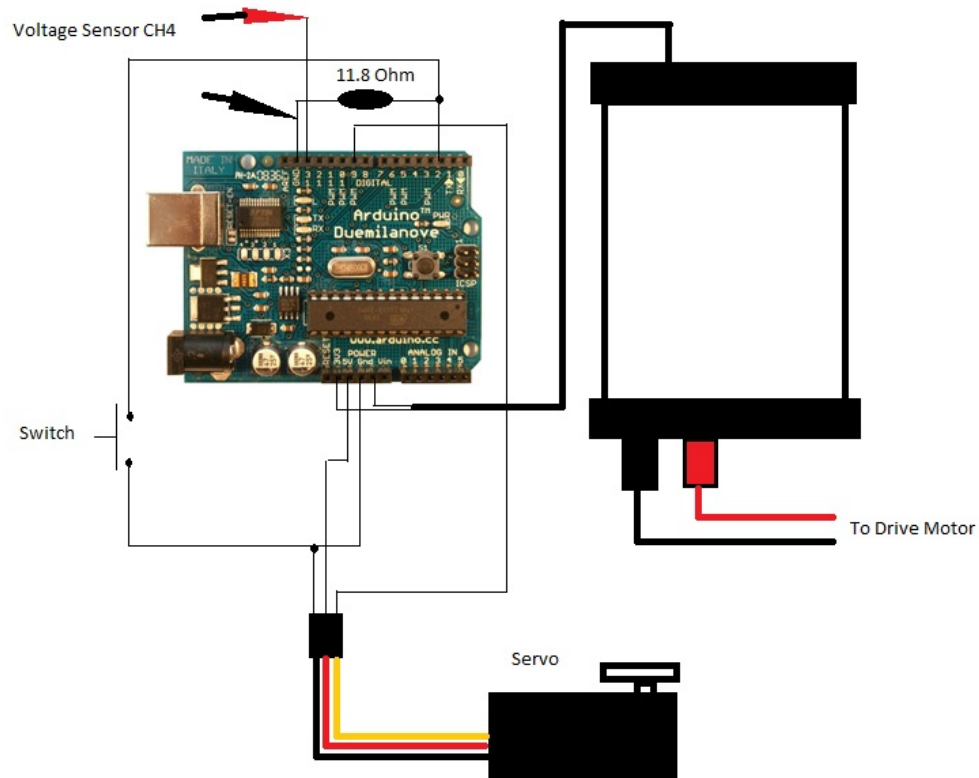


Figure 9 - Circuit diagram

### *Program*

As stated in the Control section, an Arduino board controls the angle of the servo. The actual code used is supplied in the appendix. The pseudo code for the control of the servo is shown below.

---

Set all variables to 0  
 Set the pin assignments for input/output

Assign input and output pins

```

Loop {
  Read Button State
  Set initial Servo Position
  If Button is Pressed {

```

```
    Pause one Second
    Set Digital Pin to HIGH to Trigger LabPro
    Pause 0.5 Seconds
    Set Trigger Pin to LOW
    While (Servo Angle < Final Angle)
        Set Servo to Angle
        Pause 10 seconds
        Increase Servo Angle by 5 degrees
    }
}
```

---

### *Procedure*

For each of the runs, the same procedure is used. The setup is shown in the circuitry section. All ports on the LabPro and the Arduino board must also be the same as illustrated for the testing device to work properly.

### *Preliminary Setup*

- The device is set on a level surface and the LabPro, Power Amplifier and the Arduino are set nearby.
- The fixed force sensor is affixed to the top ring of the testing device.
- The selected capstan is placed on the shaft of the motor and is tightened down with an Allen wrench so that the capstan will move freely but there is not enough space between the capstan and the disc for the cord to get caught.
- The servo platform is moved about the top disc of the testing device and oriented with the desired testing angle. Angle measurements are taken with a protractor.

- A new cord is measured and loops made on both ends to loop over the hooks on both of the force sensors. (A new cord is made for each angle)
- Making sure there is slack on both sides of the capstan, the two force sensors are zeroed from the LabPro acquisition software.
- The Power Amplifier is turned on and the servo tension bolt is tightened until there is approximately 0.1 N of force being read from the force sensor attached to the servo.
- Under the “Data Collection” setup box in Logger Pro, the following parameters are set for the Testing
  - Mode: Time Based
  - Length: 140 Seconds
  - Sampling rate: 30 samples/Second
  - Triggering is enabled
    - Trigger is set to “On Sensor Value”
    - Under the “Start Data Collection When” dialogue box the “LabPro: 1 CH4: Voltage (+/-10V)” is selected as the triggering sensor.
    - The trigger is set to increasing and set to activate when greater than 2V.
  - All other settings are default.
- Finally, a check is performed to make sure all devices are on and all connections are properly made and the capstan is rotating.

### *Testing*

- The “Collect” button is selected in the Logger Pro software which then displays that it is waiting for trigger data.
- Depress the trigger button attached to the Arduino.
- The servo will incrementally increase its angle and force will increase on both sensors.
- The test run is complete when the Logger Pro software shows it saving the run data.
- The testing proceeds with another run by again selecting the “Collect” button.
- A dialogue box will appear, and select “Store Latest Run.”
- For each angle a total of six (6) runs are collected.

### *Processing*

- Once all six runs have been completed the data is exported as a text file from the “File” menu.
- A spreadsheet is opened and the data is imported.
- An additional spreadsheet for the conditioned data is opened in Microsoft Excel.
- Data pairs are created by averaging from 2 seconds after the force was changed to 1 second until the force changes again for a total of 7 seconds of averaging which corresponds to 210 samples being averaged.

- This averaging is done for all steps in the sampling process with the exception of the first and last steps for a total of 12 pairs of data per run. For every angle run set there should be 72 data pairs.
- From the conditioned data, graphs and evaluations can then be made.

### Results

The raw data produced by the testing runs can be acquired upon request. The more meaningful data is the conditioned results which can be found in the appendix. This data is shown in Figure 10 and Figure 11 for both the 0.5" diameter and the 1.0" diameter shafts respectively.

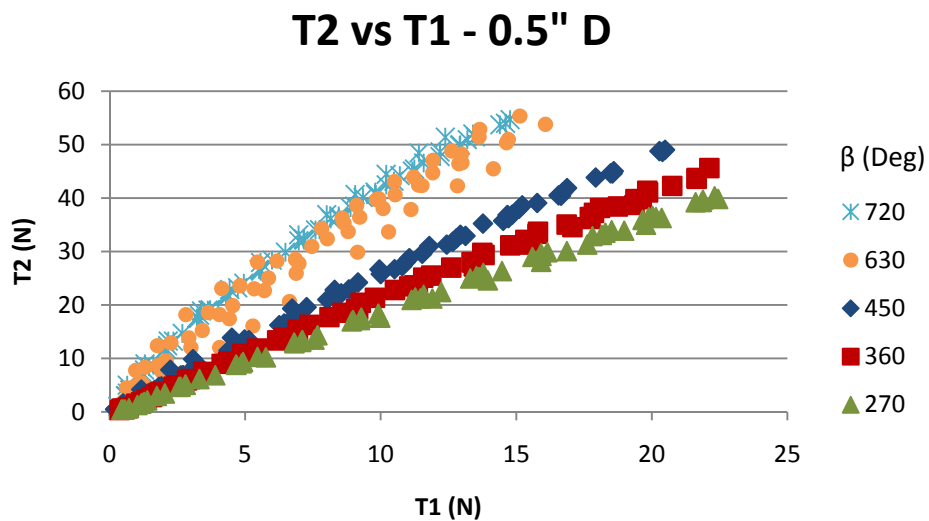


Figure 10 - T2 vs T1 - 0.5" Diameter

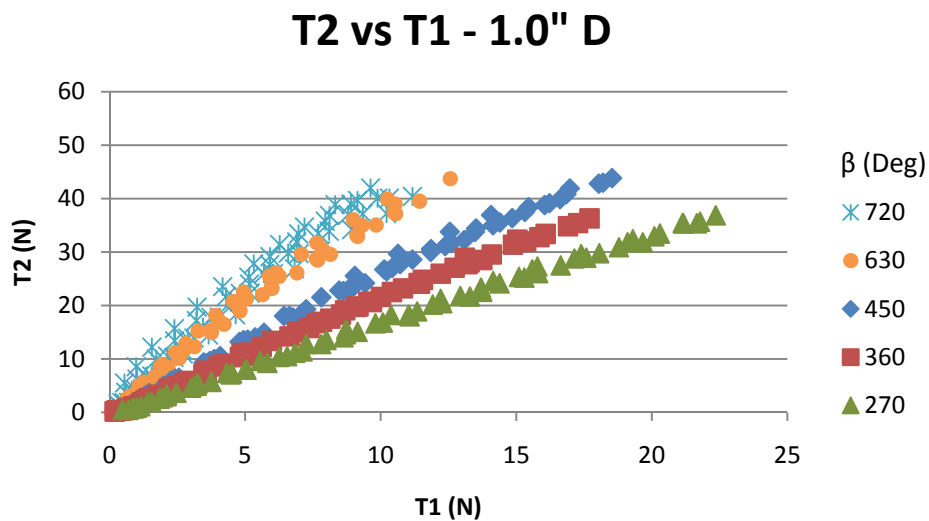


Figure 11 - T2 vs T1 - 1.0" Diameter

#### *Diameter Consideration*

The belt friction equation does not take into consideration the shaft diameter. Therefore, the data sets for each of the angle runs should coincide. To observe the correlation between the individual runs, the runs at each angle were plotted against each other.

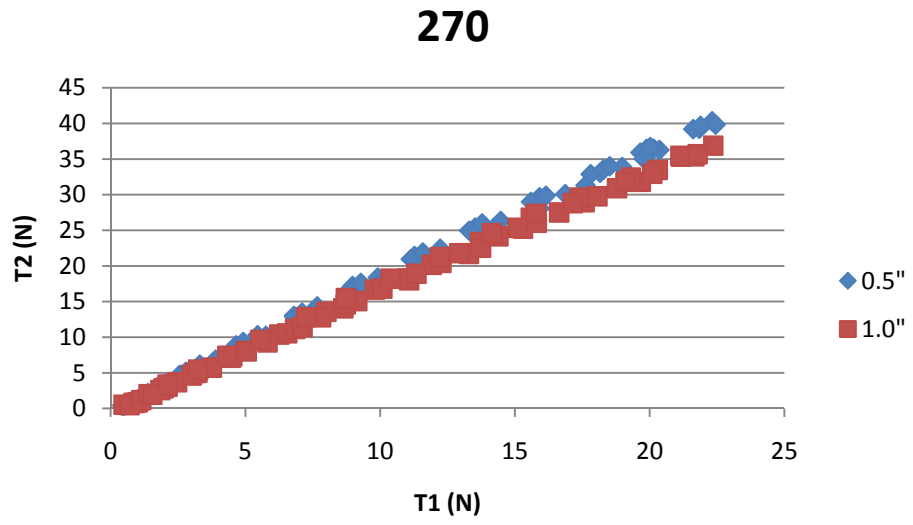


Figure 12 - 270 Degree run comparison

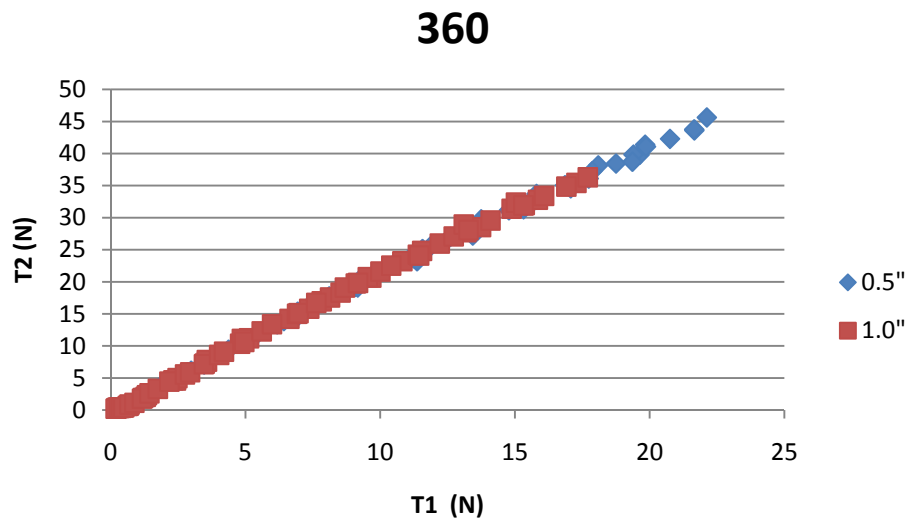


Figure 13 - 360 Degree run comparison

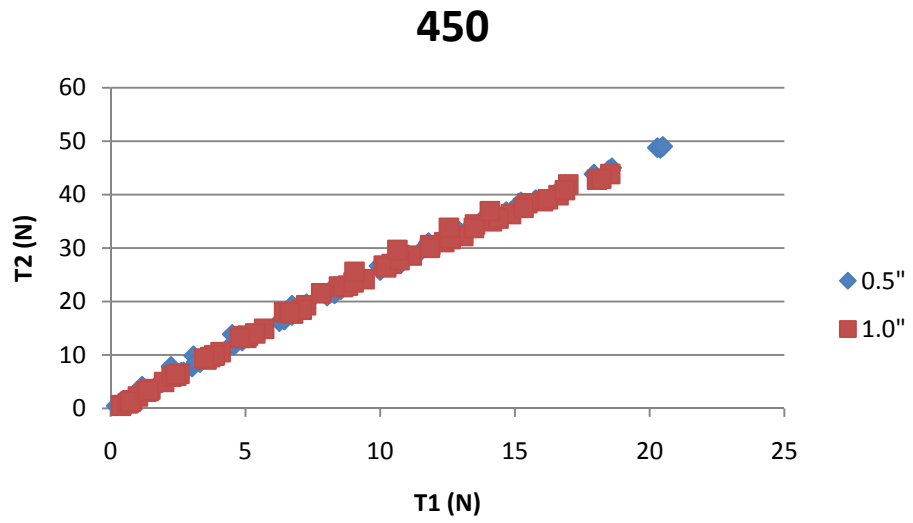


Figure 14 - 450 Degree run comparison

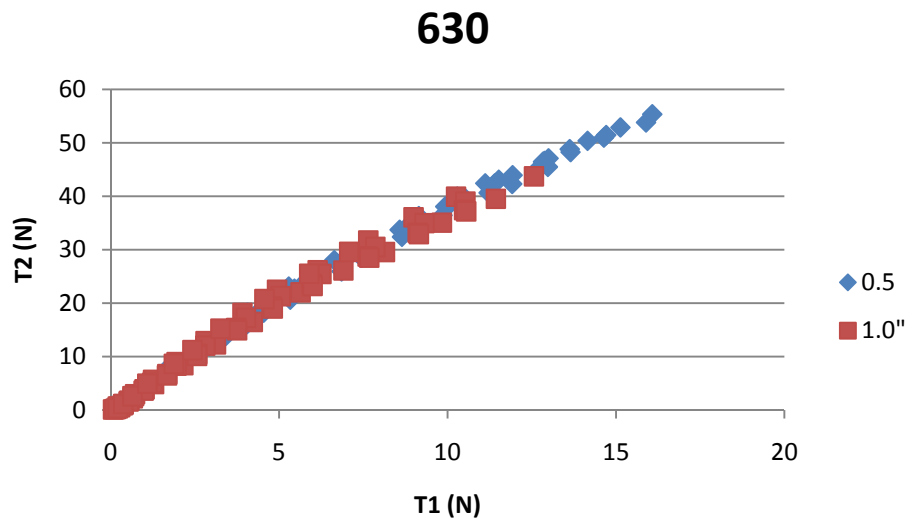


Figure 15 - 630 Degree run comparison

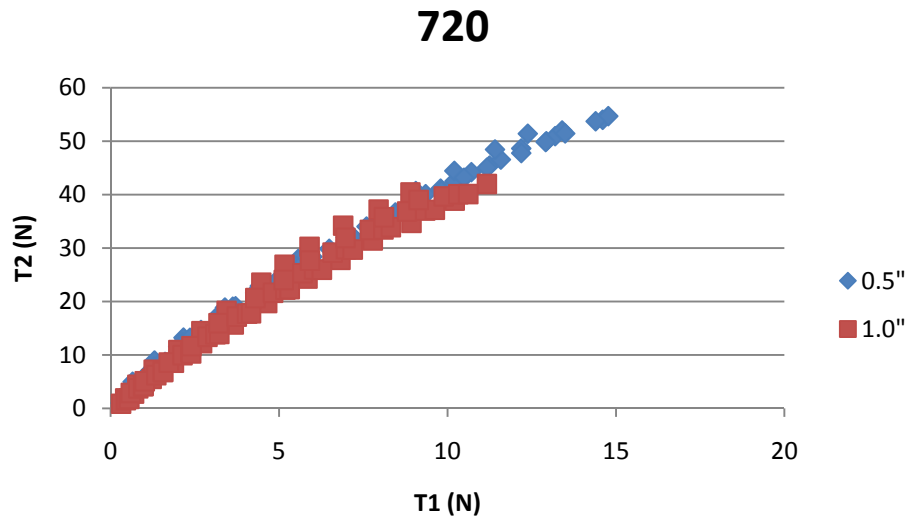


Figure 16 - 720 Degree run comparison

With the exception of the 270 degree and 720 degree runs, there is a high degree of correlation. In regards to the 270 degree run, the data for the 1.0 inch diameter shaft is slightly below the 0.5 inch. The reason for this discrepancy is not known. The 720 data has a high degree of correlation but the data for the 1.0 inch is noisy. It can however be seen that the average trend seems to follow the less noisy 0.5 inch data.

#### *Angular Velocity Consideration*

The rotational speed of the shaft is another term which is left out of Equation 1. If the belt friction equation is to hold up, the data should remain the same even when the shaft speed is changed. The initial tests were conducted at a 10V supply given to the drive motor. To check the dependence on shaft rotational speed, the voltage was increased to 20V, which from DC motor theory causes an increase in rotation speed. The

experiments were carried out the same as with the previous data, but for the rotational comparison, only the 1.0 inch shaft was used. The direct comparisons for the 360, 450, 630 and 720 degree tests are shown in Figure 17, Figure 18, Figure 19 and Figure 20 respectively.

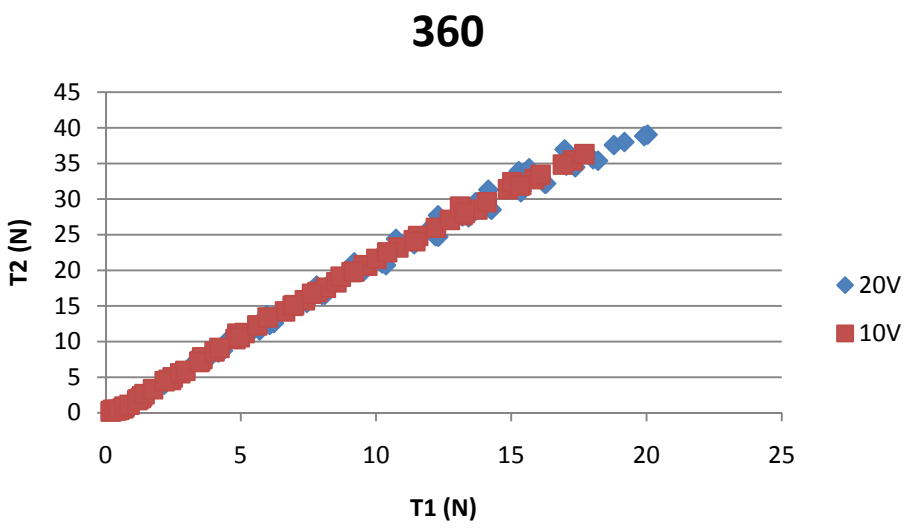


Figure 17 - 360 Degree rotational speed comparison

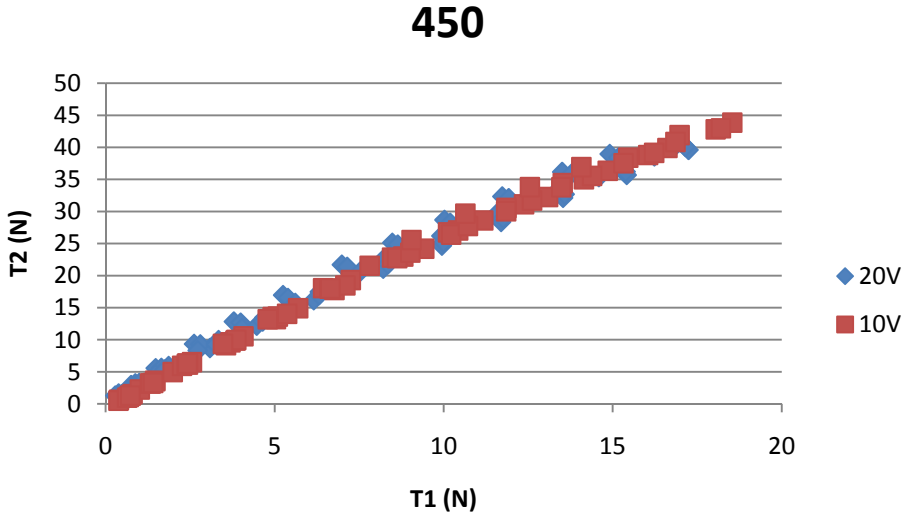


Figure 18 - 450 Degree rotational speed comparison

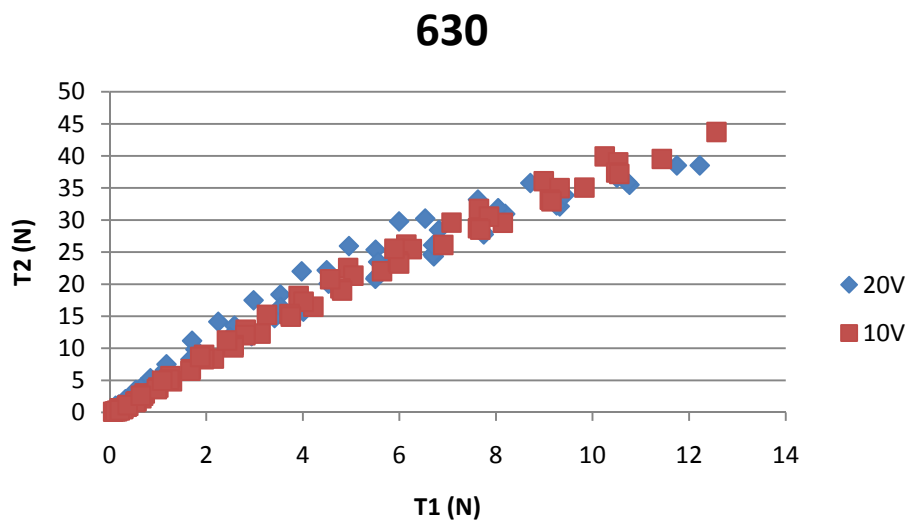


Figure 19 - 630 Degree rotational speed comparison

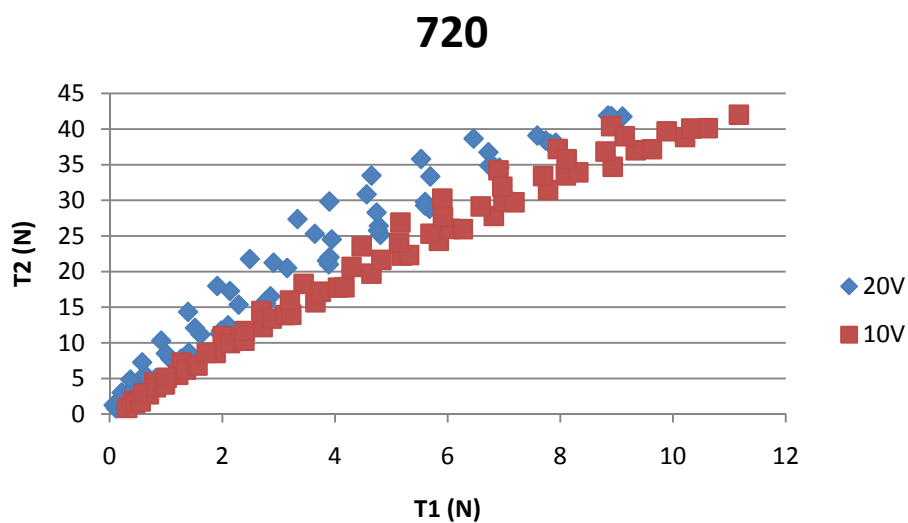


Figure 20 - 720 Degree rotational speed comparison

Aside from the 720 degree run which displays a high degree of variance and a slight divergence of the data, the runs at different rotational speeds produced similar

results. The results from the 1.0 inch test showed a good correlation between the data sets and since in the previous section it was determined that the shaft diameter did not play a role in the amplification result, the 0.5 inch trials were not conducted.

### *Belt Friction Adherence*

The main question which arises from the data is if it follows the belt friction equation. To check the correlation, theoretical lines representing the belt friction equation were laid over the experimental data. These plots can be seen in Figure 21 and Figure 22. The values used for the friction variable in the belt friction are shown in Table 1. It appears that the belt friction equation holds true and the data are following it. The capstan equation is plotted against the experimental data to show correlation and is abbreviated in the plots as “E Fit” because of the exponential behavior of the underlying equation.

**Table 1 - Friction values for exponential fit**

Run	0.5"	1.0"
270	0.12	0.11
360	0.115	0.115
450	0.115	0.115
630	0.115	0.115
720	0.115	0.12

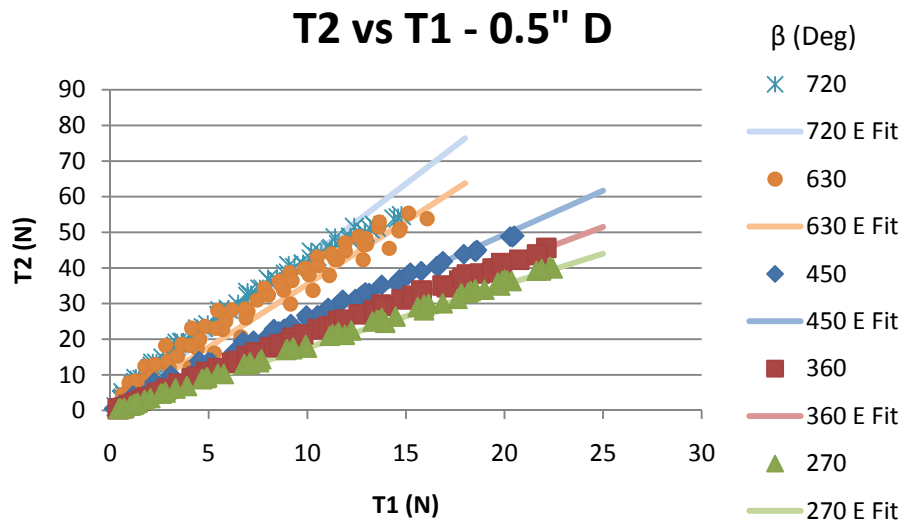


Figure 21 - T2 vs T1 - 0.5" Diameter with capstan equation curve fit

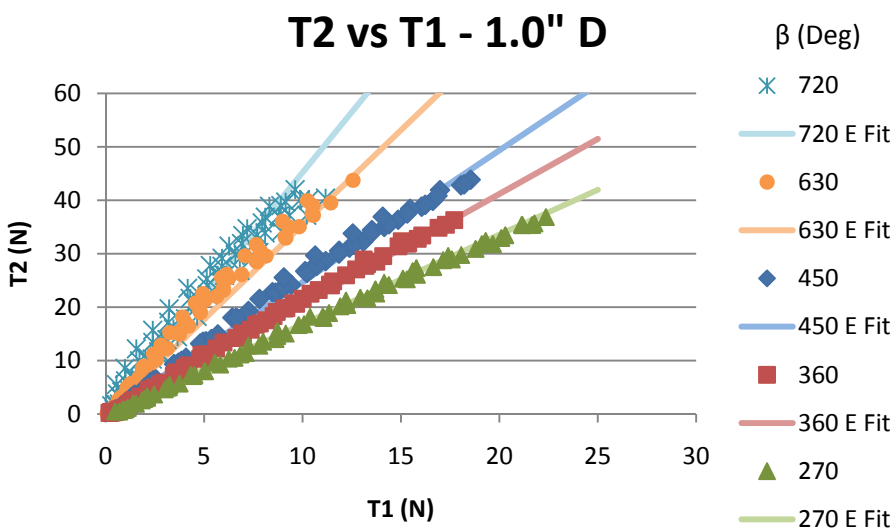


Figure 22 - T2 vs T1 - 1.0" Diameter with capstan equation curve fit

For both of the plots, the data seems to adhere to the belt friction equation.

Referencing back to the correlation plots (Figure 12, Figure 13, Figure 14, Figure 15 and

Figure 16) however, it is seen that even though the plots for 270 degrees and 360 degrees seem linear, the plots for the higher angles show a noticeable degradation. To determine what type of degradation is occurring, the amplification (the ratio of  $T_2/T_1$ ) for the two data sets is plotted in Figure 23 and Figure 24. Amplification occurs in the belt friction equation in the exponential and remains constant unless either the friction or the angle change, neither of which are changed during an experimental run.

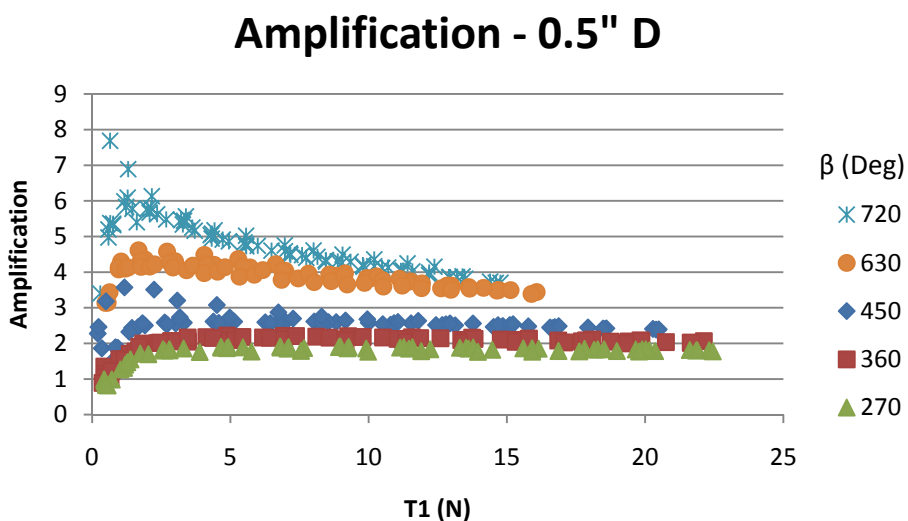


Figure 23 - Plot of Amplification ( $T_2/T_1$ ) - 0.5" Diameter

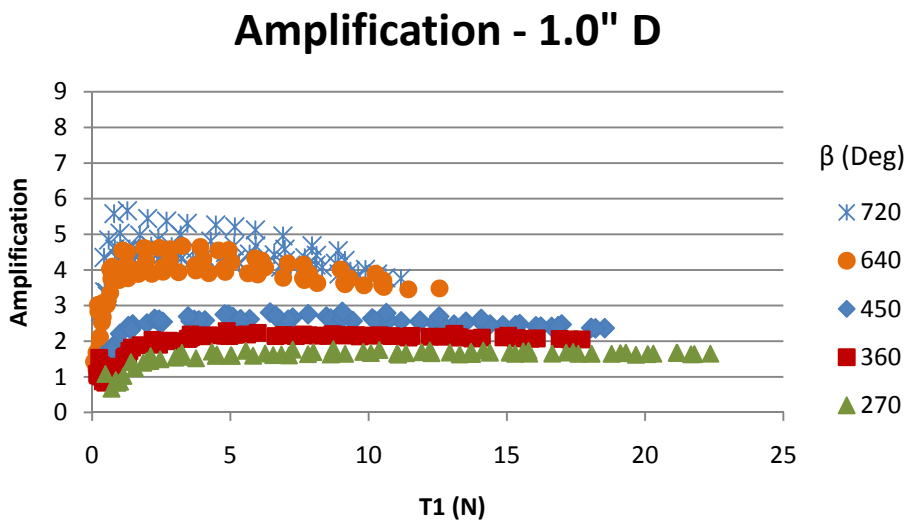


Figure 24 - Plot of Amplification ( $T_2/T_1$ ) - 1.0" Diameter

If the data had adhered to the belt friction equation, the amplification for the test data should resemble that of Figure 25 and Figure 26 and remain constant over all input tensions. Instead there is a distinct pattern shown in both of the data sets which includes a brief increase followed by a gradual decrement.

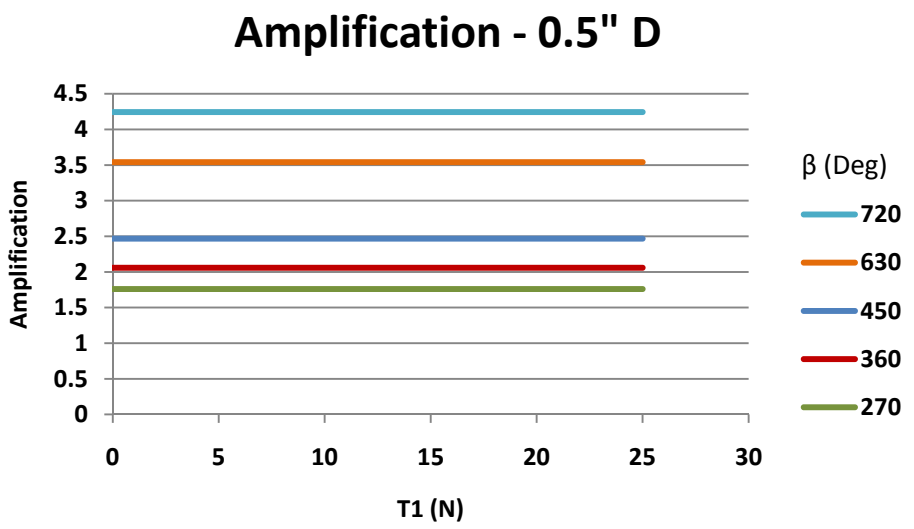


Figure 25 - Theoretical amplification curves for capstan equation – 0.5" Diameter

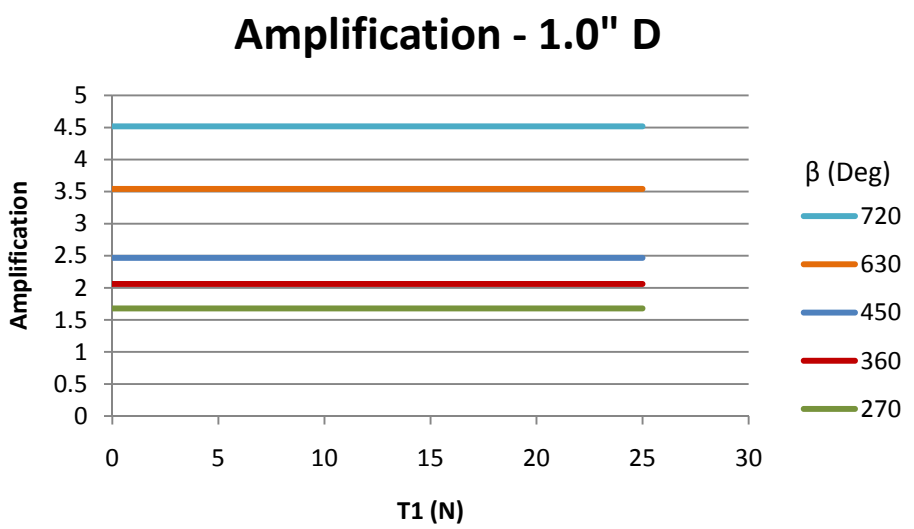


Figure 26 - Theoretical amplification curves for capstan equation - 1.0" Diameter

To acquire a better understanding of the amplification trends, I separated each of the angles and compared them between the 0.5 inch and 1.0 inch runs. As with the plots

comparing the input tension T1 to the output tension T2, there is a high correlation between the 0.5 inch data and the 1.0 inch data. The two data sets for the 270 degree tests were off still which is to be expected and the data for the 720 degree runs show a better average correlation.

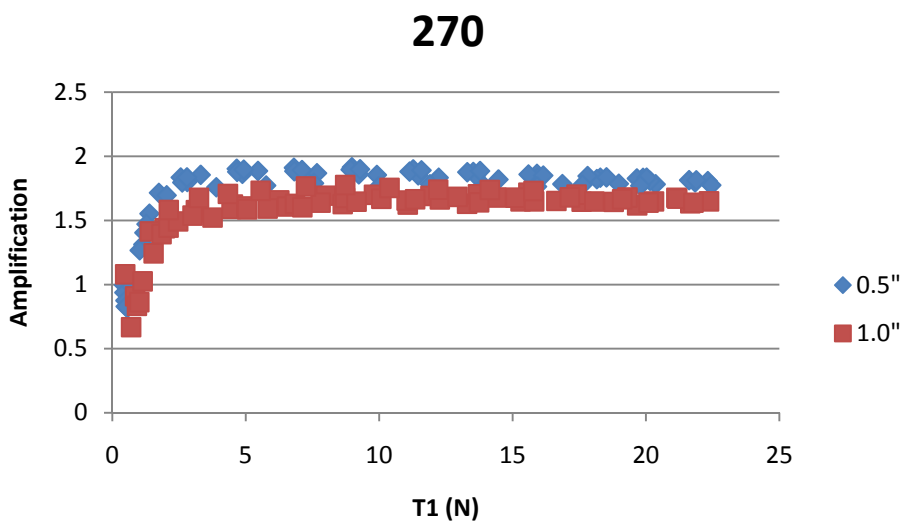


Figure 27 - Amplification comparison at 270 degrees

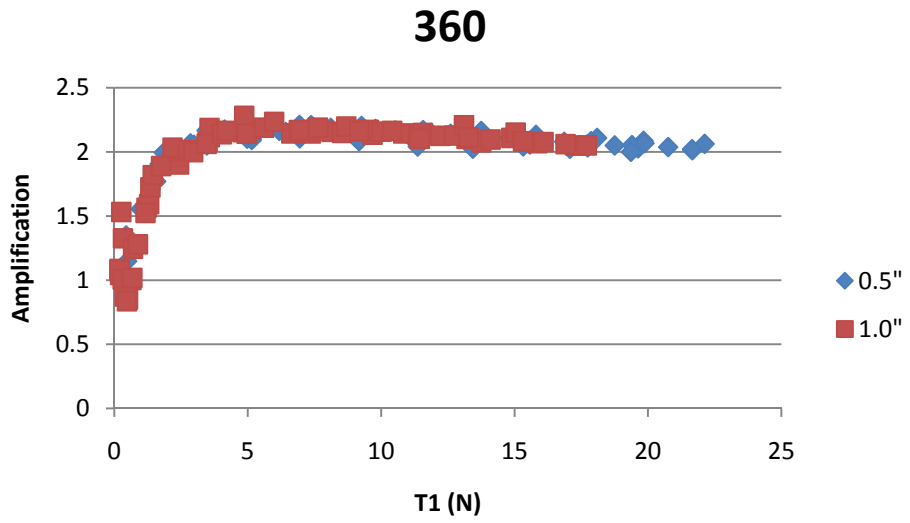


Figure 28 - Amplification comparison at 360 degrees

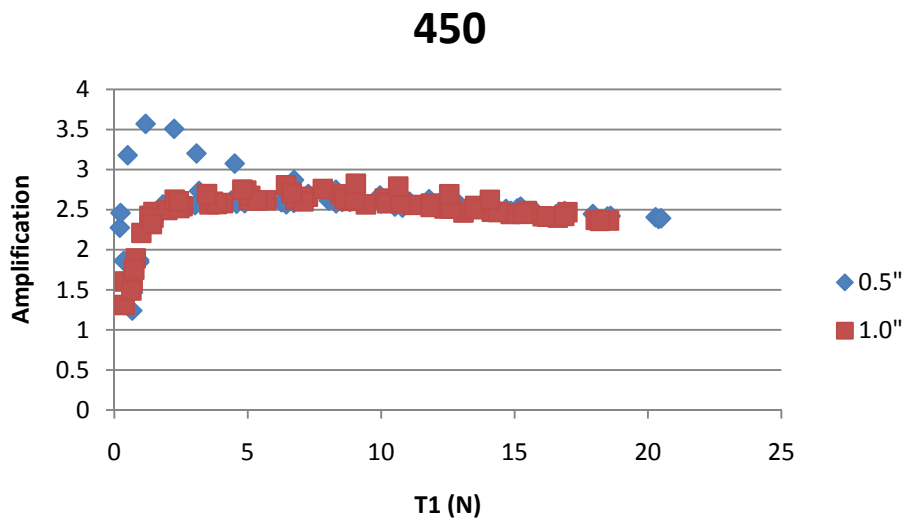


Figure 29 - Amplification comparison at 450 degrees

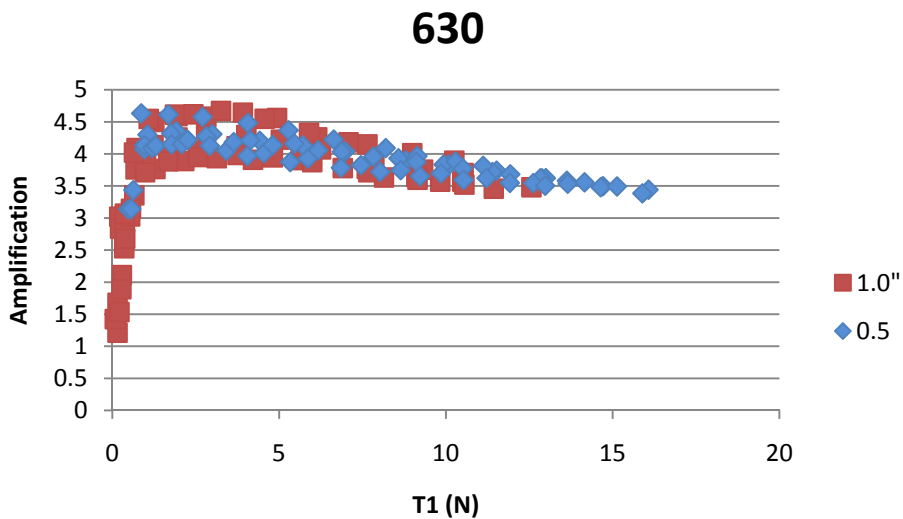


Figure 30 - Amplification comparison at 630 degrees

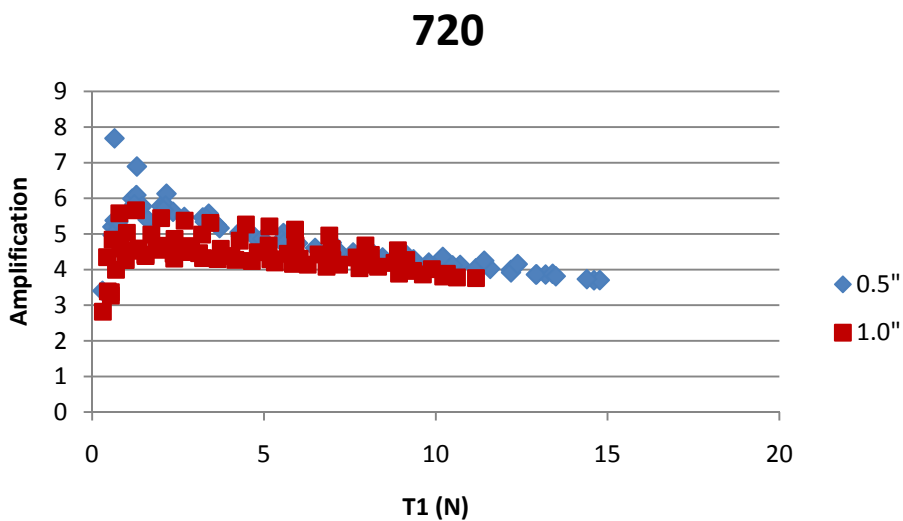


Figure 31 - Amplification comparison at 720 degrees

From observing the data from the amplification, there are two distinct regions to the data sets which are shared between each of the runs. There is a sharply increasing

initial region followed by a slow decay. To fit an equation to the data the two portions will be dealt with separately. It is hypothesized that the rapidly increasing initial region is due to a settling phenomena, which will be discussed later, and the following slow decreasing region is hypothesized to be attributed a diminishing returns effect on the ability for the developed friction to create tension in the cord.

To model the slow region, an appropriate curve needed to be chosen as a model curve to fit to the data. A basic exponential decay function, shown in Equation 10, was used since the shape of the function resembles the curves made from the data.

$$f(x) = N_0 e^{-\lambda x} + SS \quad (10)$$

The exponential decay function has three assignable variables. The SS term corresponds with the steady state of the function which is the value at which the function reaches when the exponential approaches a value of zero, if the equation dealt with a time based x value, the SS value would be considered the value the equation would reach when the time was infinity. There are two variables which modify the exponential,  $N_0$  determining the transient magnitude of displacement and  $\lambda$  as the rate of decay.

For each of the pairs of data, Equation 10 was assigned different values for the three terms to find the best fit to the experimental curve. These values are shown in Table 2. For the following plots, the fitted curve is shown by the black lines.

Table 2 - Exponential decay variables used for curve fitting

Angle (deg)	270	360	450	630	720
SS	1.75	2	2.3	3.1	3.4
No	0.25	0.5	1	1.8	2.5
$\lambda$	0.11	0.11	0.11	0.11	0.11

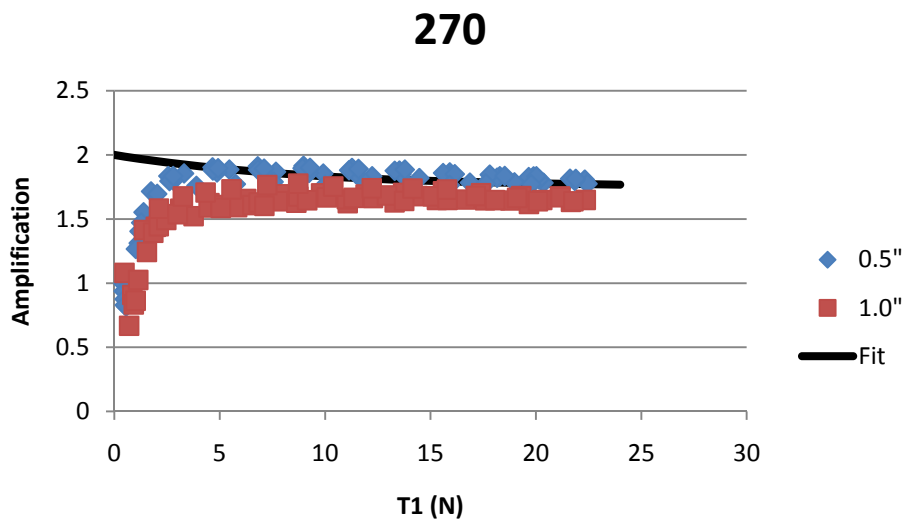


Figure 32 - 270 degree - amplification fit - exponential decay

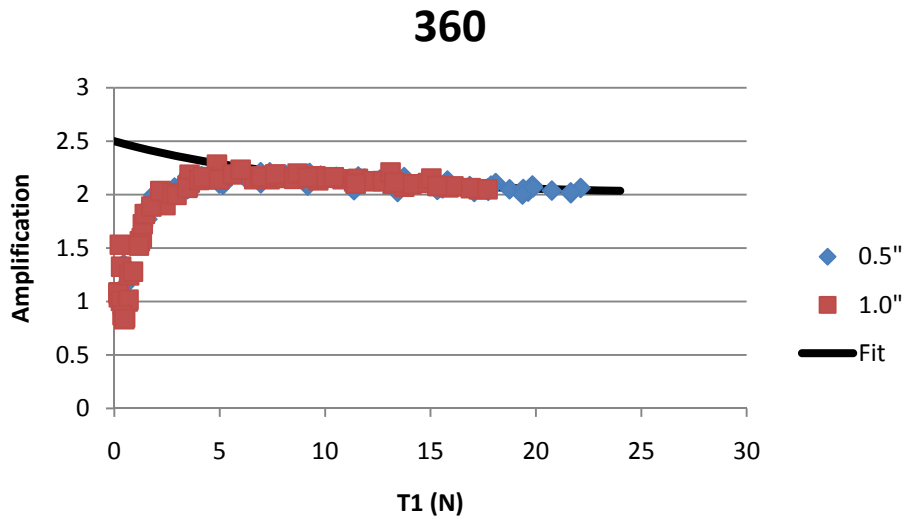


Figure 33 - 360 degree - amplification fit - exponential decay

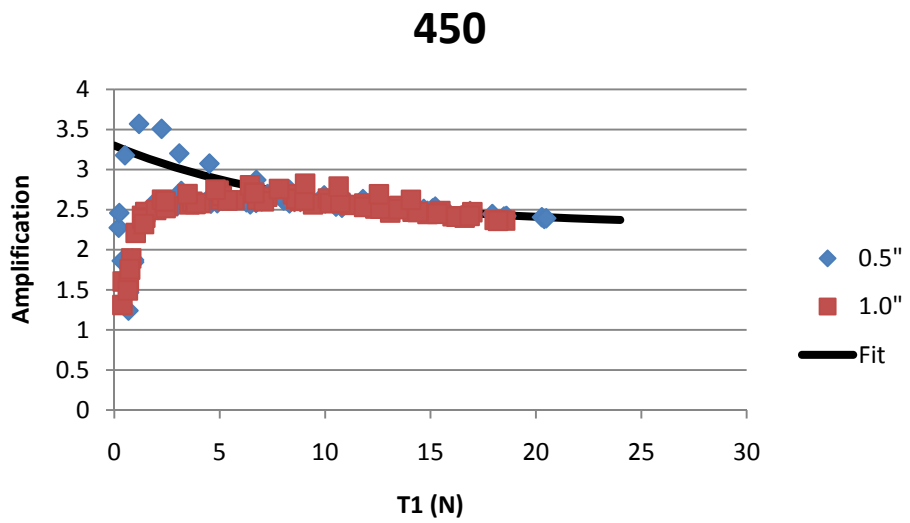


Figure 34 - 450 degree - amplification fit - exponential decay

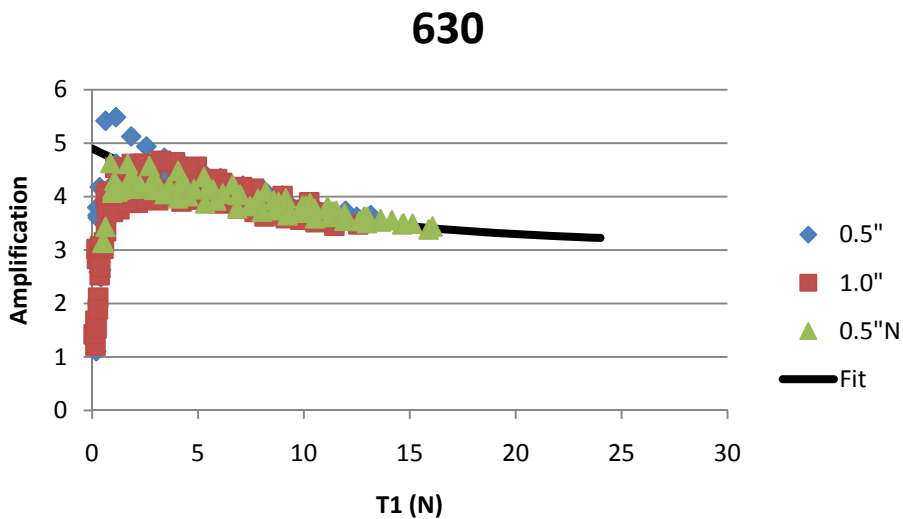


Figure 35 - 630 degree - amplification fit - exponential decay

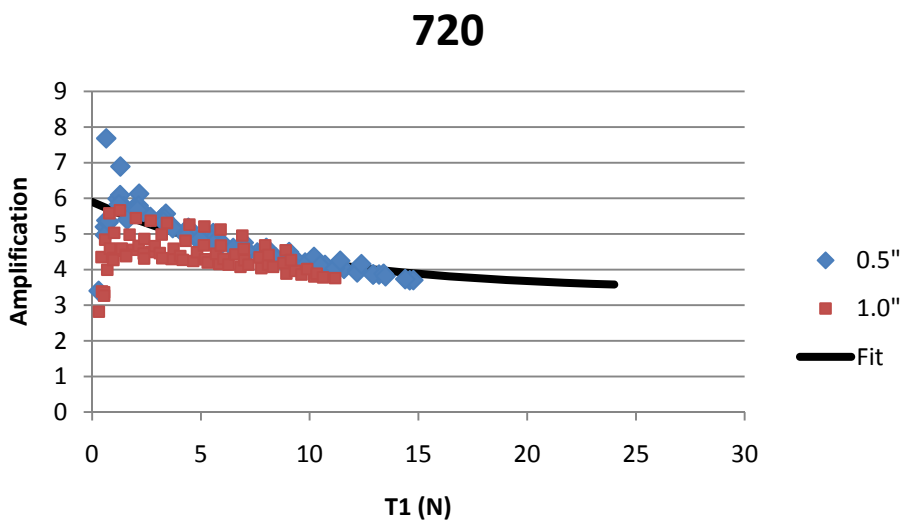


Figure 36 - 720 degree - amplification fit - exponential decay

It can be seen from the figures that the exponential decay function fits well with the slow decreasing region on each of the plots. A first observation of possible correlation

was the fact that each of the curves possessed the same value for lambda. The curves were fitted via visual inspection so the fact that all of the lambda terms are equal could simply be a coincidence. To get a better understanding of correlation between the graphs and to determine if there were any possible correlations or trends appearing, the values for the No and SS term were plotted (shown in Figure 37 and Figure 38).

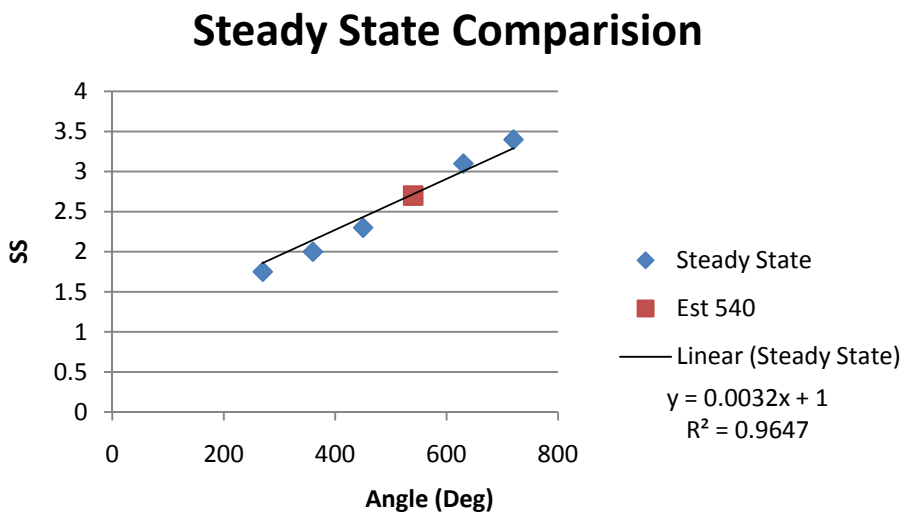


Figure 37 - Comparison between angle of contact and SS term of the exponential

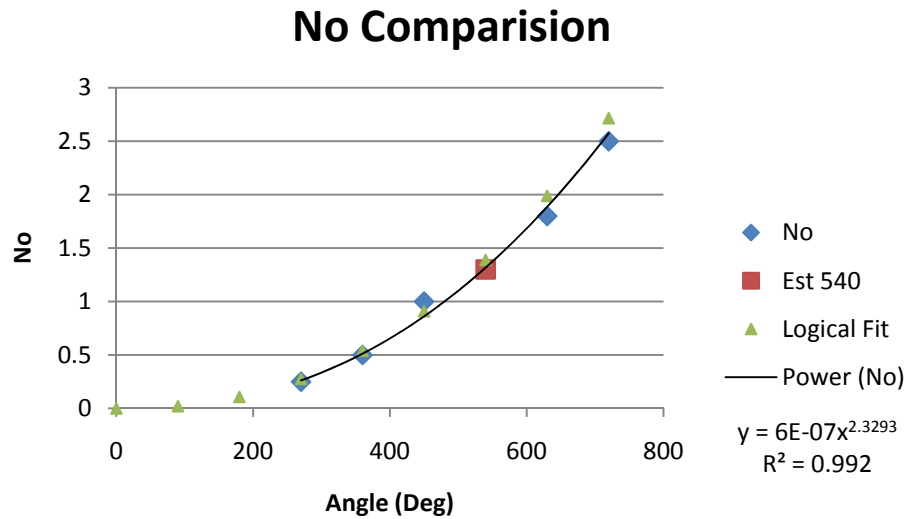


Figure 38 - Comparison between angle of contact and No term of the exponential

The blue diamonds in Figure 37 are the values obtained from the experimental data. It can be seen that the experimental data appears to be following a linear trend. A line was fitted to the data and is shown on the plot. An automatic fit of the line to the data produces differing results than what are shown in the figure. The reason why the linear fit in the plot is different is because it is crucial that the data be fitted to a line which has a y-intercept at 1. When examining Equation 10, it is obvious that any intercept other than one will cause the system to produce an amplification at zero contact angle, which is impossible. The data for the No variable has a similar constraint as with the steady state curve. If Equation 10 is to be assumed correct, any function which solves for No will have to produce a value of zero at a zero contact angle. Otherwise, the system would have the same error of false amplification. A power function was chosen because of its adherence to the constraint and fit to the data. From the two variable plots, the values for

a 540 degree run were estimated. All of the fitted curves were plotted and shown in Figure 39.

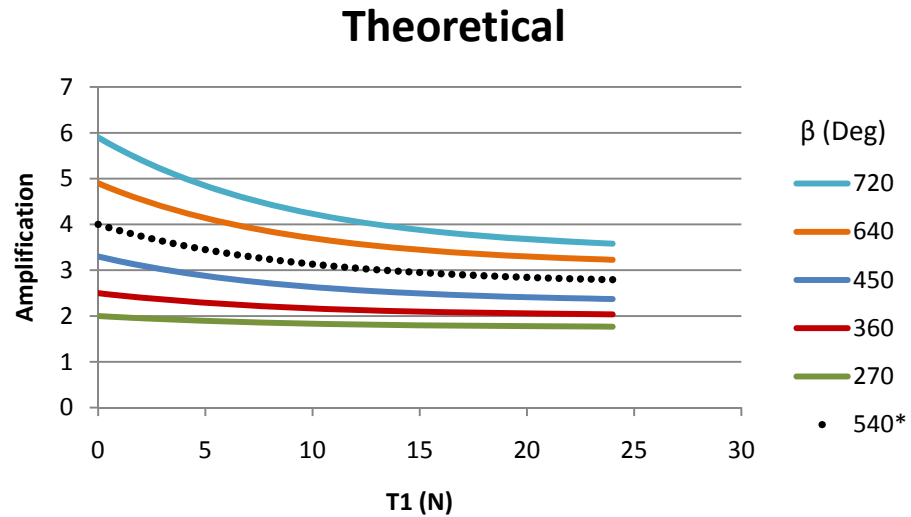


Figure 39 - Slow decrement region plot comparison between angles of contact

Comparing the results with Figure 23 and Figure 24 it can be seen that all three of the plots share similar shapes within the slow decrement region. The portion of the equation missing is that which deals with the fast rising region. If the slow decay region is assumed to be a correct representation of the idea function for amplification, it can be assumed that there is some factor which is resisting the ability for the system to develop the amplification. This effect will be treated as an addition factor which is similar to Equation 10 in the fact that it is a standard exponential, however the steady state will be replaced by Equation 1 resulting in Equation 11.

$$f(x) = -N_d e^{-\lambda_d x} + N_0 e^{-\lambda x} + SS \quad (11)$$

The same process for fitting the new curve was used as was used for the slow decay region. Numbers were assigned to the curves in order to visually fit them to the experimental data. The new variables are shown in Table 3.

**Table 3 - Double exponential full curve variables**

Angle (deg)	270	360	450	630	720	*540
SS	1.75	2	2.3	3.1	3.4	4
No	0.25	0.5	1.0	1.8	2.5	1.3
$\lambda$	0.11	0.11	0.11	0.11	0.11	0.11
$N_d$	2	2.5	3.3	4.9	5.9	2.7
$\lambda_d$	0.6	0.7	0.9	1.5	2	1.17

The resulting plots developed by the variables inserted into Equation 11 are shown in the following.

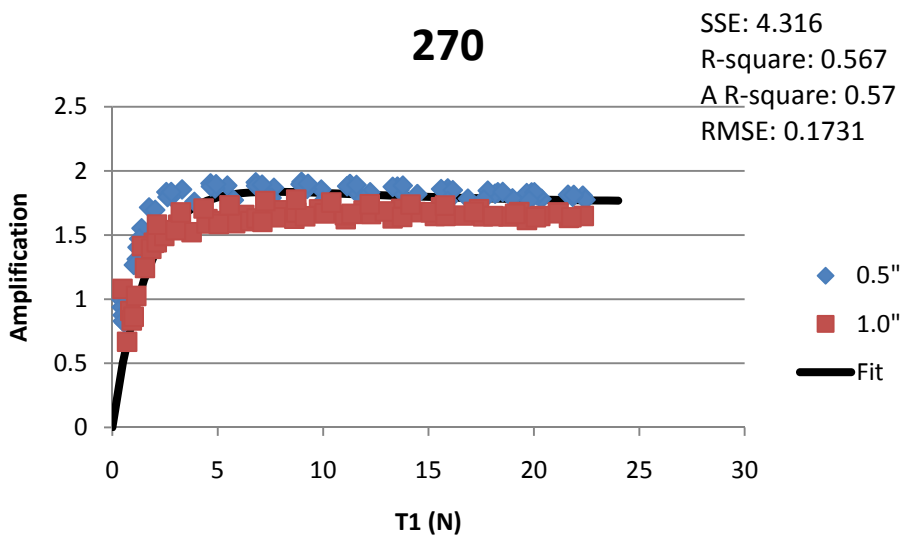


Figure 40 - Double exponential full curve fit - 270 degrees

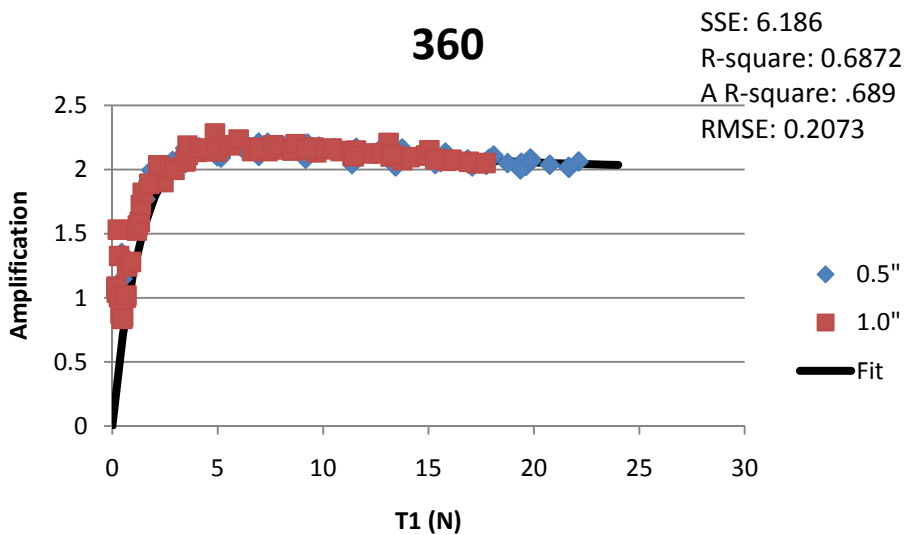


Figure 41 - Double exponential full curve fit - 360 degrees

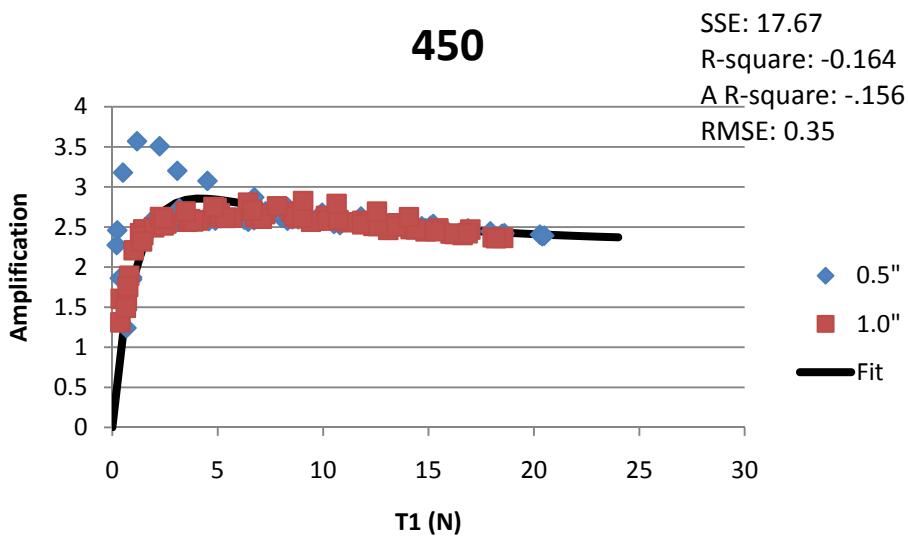


Figure 42 - Double exponential full curve fit - 450 degrees

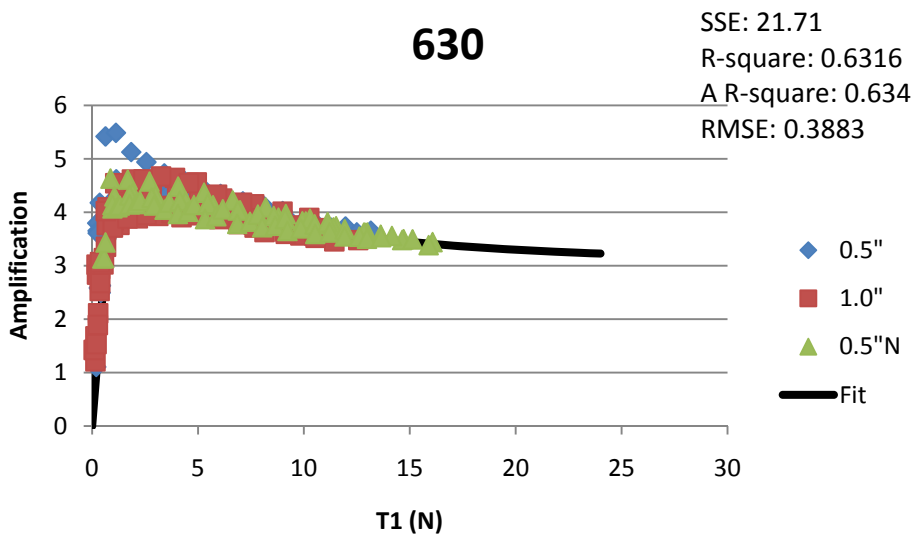


Figure 43 - Double exponential full curve fit - 630 degrees

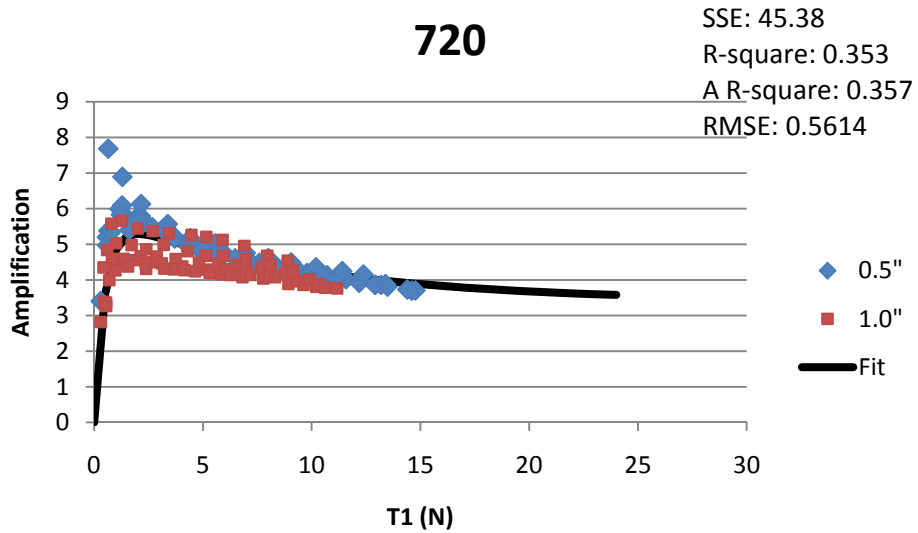


Figure 44 - Double exponential full curve fit - 720 degrees

After fitting each of the data sets with the curve defined by Equation 11, it can be noted that in each case the curve was able to follow the data and conform to the shape. For each of the fitted curves, goodness-of-fit statistics were evaluated to determine the ability for the double exponential equation to estimate the data. The statistics were performed using the curve fitting toolbox for MATLAB and the definitions for the terms and the methodology for calculating them is available from the toolbox help.

The SSE (Sum of Squares due to Error) is a measure of the total deviation the data has from the fitted curve and offers a prediction of the ability for the curve to predict the data. A value as close to 0 is ideal (MATLAB n.d.). Each of the data plots show relatively low SSE values which exhibit a trend of becoming larger which reflects the trend of increasing noise.

The R-square and Adjusted R-square (A R-square) are measures of the square of correlation between the fitted plots and the data. For example, the curve for the 360 degree data has an r-square value of 0.687 which translates to the curve being able to describe 68.7% of the variation in the data about the average. A value of 1 is desired and the values found range from a negative to 0.687. The negative suggests that the calculation requires a constant term which alludes to a horizontal line being better than the fit. The adjusted r-square calculation adjusts the r-square with respect to the number of degrees of freedom. (MATLAB n.d.)

The final statistic is the root mean squared error (RMSE) which is a measure of the standard deviation of the data. A value closer to 0 predicts the data is useful for predicting the behavior of the data (MATLAB n.d.). All of the values found for the curves were close to 0 with the common trend of increase due to the increase in noise from the data.

Similar to the previous case, the two additional variables were plotted to determine common trends and to attempt to estimate a value for the 540 degree run.

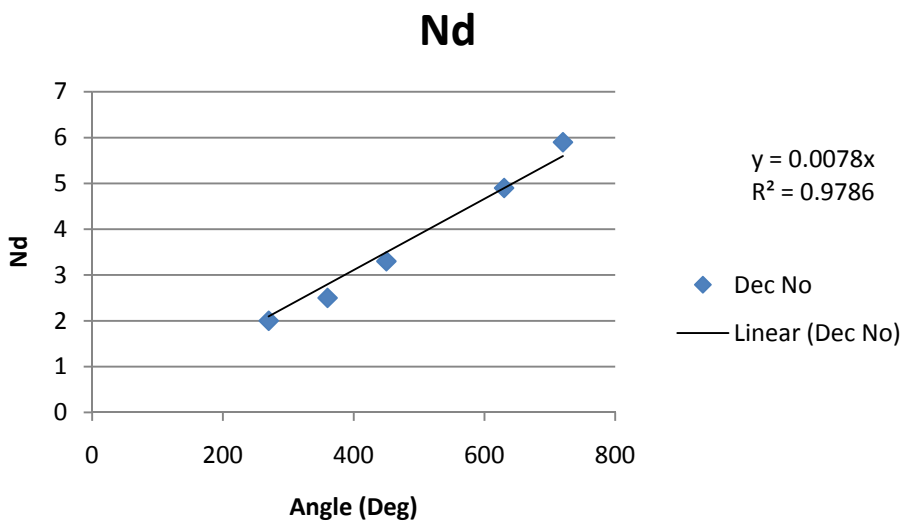


Figure 45 - Relationship between Nd term of the double exponential and the angle of contact

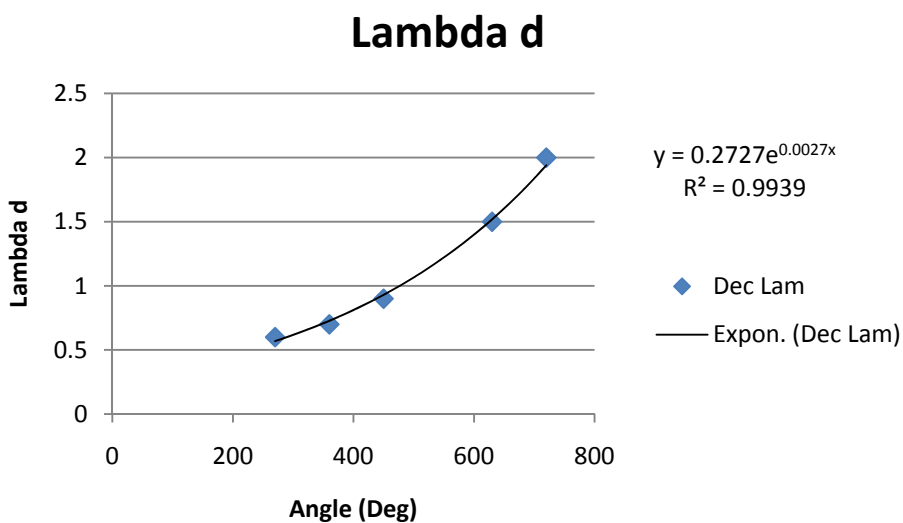


Figure 46 - Relationship between the Lambda d term of the double exponential and the angle of contact

Care had to be taken when choosing the appropriate fit for the data of Nd for the same reasoning as with No. The same constraint of having an intercept at 0 applies to Nd

for the same reasons. The plot for the  $\lambda_d$  term provided useful information as to the rate of increase for the short increasing region. After plotting the data, an exponential function was fitted. The good correlation allowed for a confident plot of the 540 degree data and allowed a full set of theoretical values to be plotted, shown in Figure 47. Referencing back to Figure 23 and Figure 24 and comparing their values to Figure 47 it is easy confirmed that the whole data sets follow the shapes for each of the plots.

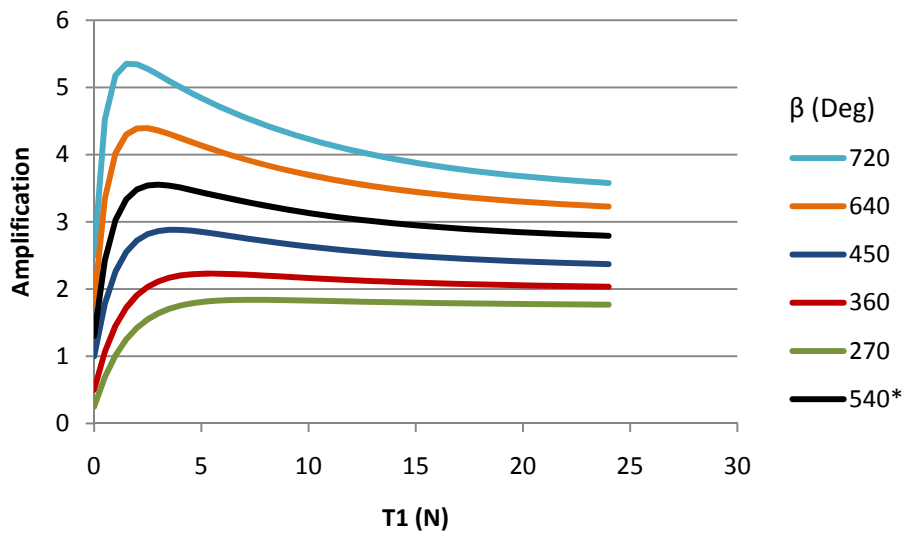


Figure 47 – Theoretical curves describing the experimental plots of amplification

After developing Equation 11 and confirming its ability to describe the estimated curves, it is necessary to determine if the application of the equation will result in accurate representation of the developed force with a force applied. Equation 11 acts as a replacement for the exponential term in Equation 1. Creating an equation that represents the force out with a given input force requires simply replacing these terms as shown in Equation 12.

$$T_2 = T_1(-N_d e^{-\lambda_d x} + N_0 e^{-\lambda x} + SS) \quad (12)$$

For the equation to hold, it must accurately predict the resulting force output given a force input. To visually assess its ability to perform, it was plotted over the experimental data shown in the following plots.

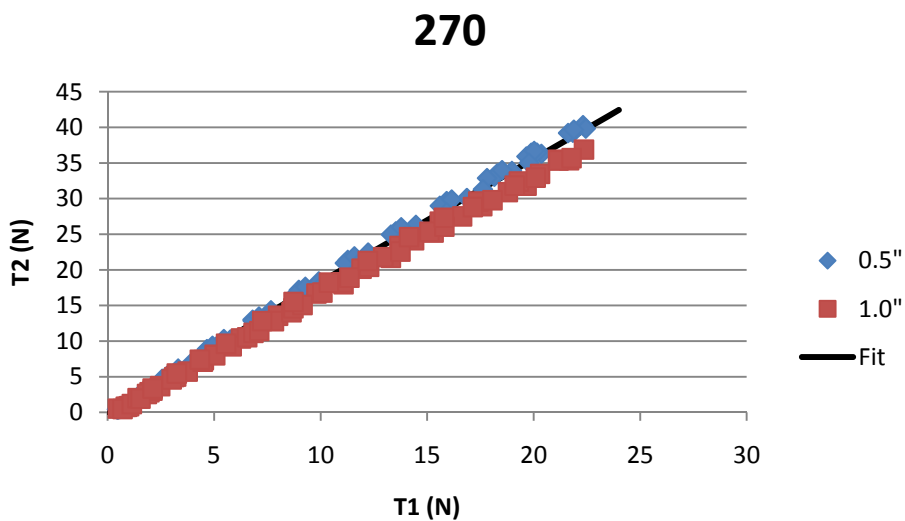


Figure 48 - Performance of double exponential fit to the experimental data - 270 degrees

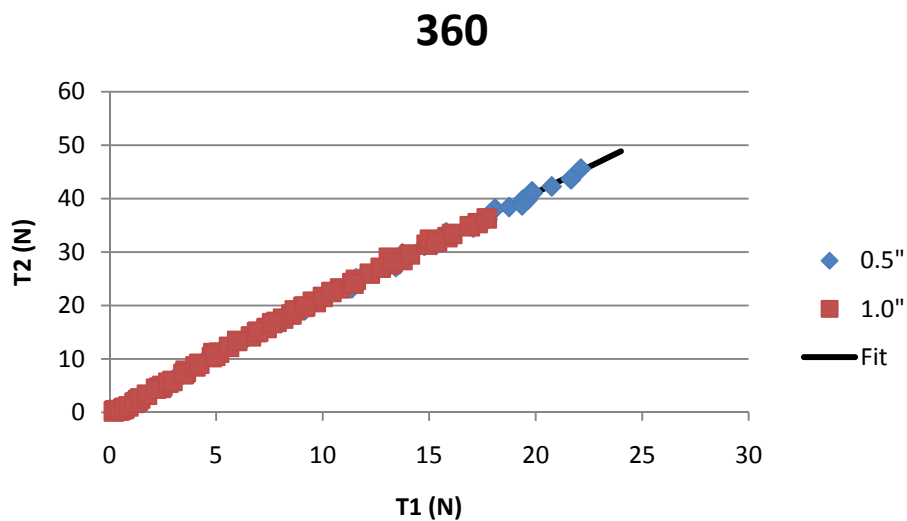


Figure 49 - Performance of double exponential fit to the experimental data - 360 degrees

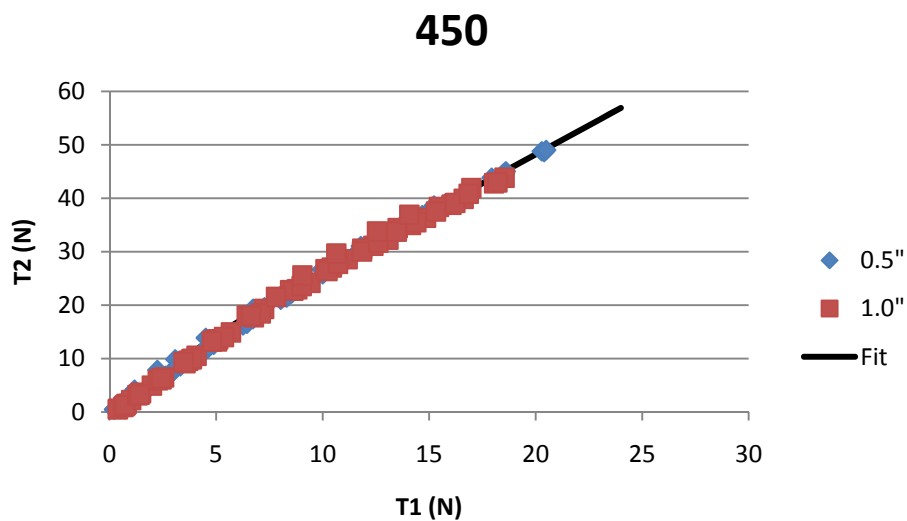


Figure 50 - Performance of double exponential fit to the experimental data - 450 degrees

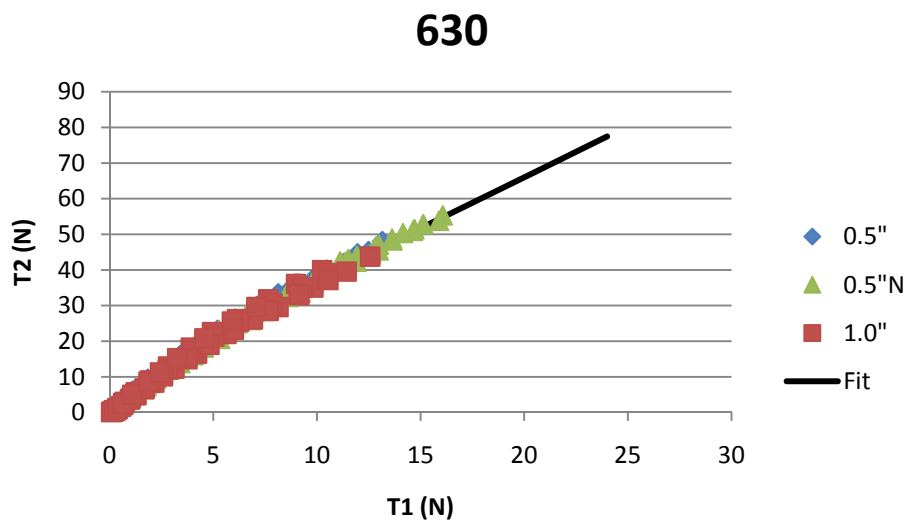


Figure 51 - Performance of double exponential fit to the experimental data - 630 degrees

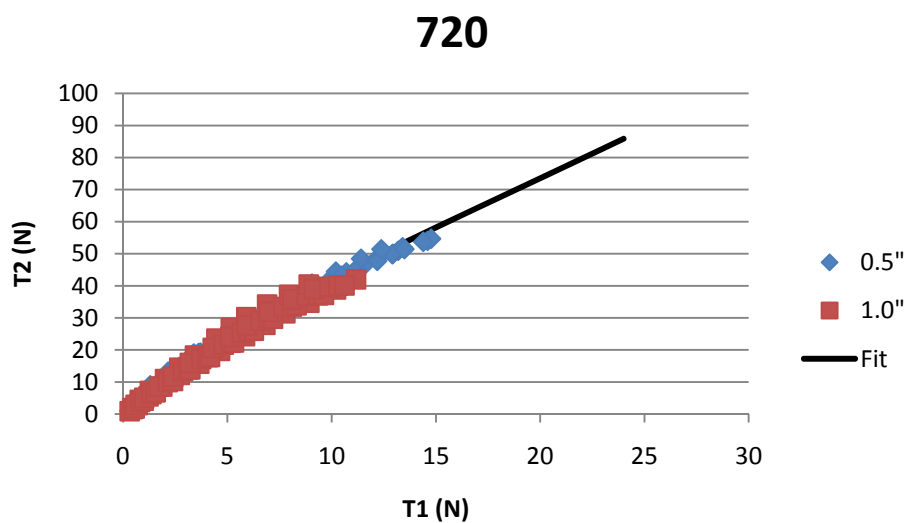


Figure 52 - Performance of double exponential fit to the experimental data - 720 degrees

For each of the plots, Equation 12 performed exactly as the data. It is then assumed that the definition of Equation 12 can accurately describe the trends which exist

in the system. The single exponential is not adequate to fully represent the system and the more complicated two part equation is needed. For reference, each of the curves in addition to the estimated value for the 540 degree run are plotted in Figure 53. The estimated curves are plotted with the experimental data for both sets attached in the appendix as Figure 61 and Figure 62.

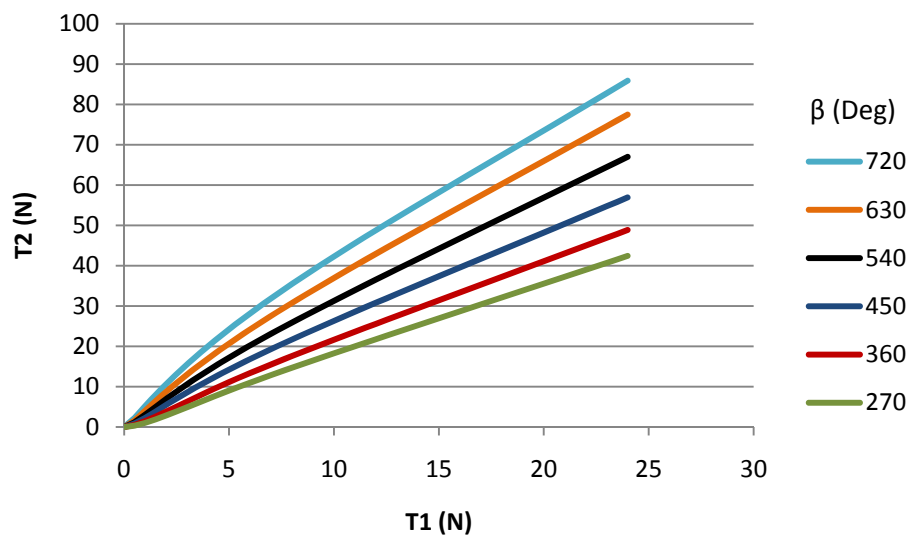


Figure 53 - Double exponential estimation curves for experimental data

### *Theory on Fast Rising Region*

The reason there is a fast rising region in the data is still unknown, however a theory has been formulated to describe what may be happening. Three cross sections of the cord wrapped around the capstan are shown in Figure 54. A cord with no tension in it could be assumed to have very little contact with the capstan surface with a cross section looking similar to section A. As tension develops in the cord, it will begin to conform to

the surface of the capstan i.e. sections B and C. With more surface area in contact with the capstan, more force is able to be transferred to the cord. In section A there would be very little friction transferred and would represent why the curves start from zero. The speed at which the cord conforms to the capstan can then be defined by the fast rising region.

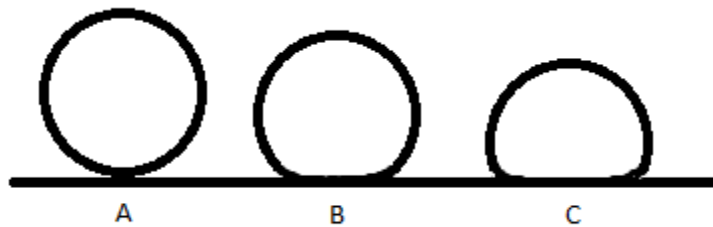


Figure 54 - Possible cord deformation causing fast rising region in data

## SIMULATION

The initial simulation was created to attempt to replicate the data produced by the experimentation. The program simulates the exact experimental setup. A rotating link, representing the servo incrementally changes direction which increases the force on the T1 sensor. The program is initiated and executed from the MATLAB m-file which works in conjunction with the Simulink model. Angle iterations are passed to the Simulink model where the values are each run are calculated and the data is returned to the workspace where the m-file assembles it into its appropriate matrices. The program will plot both the direct comparison values and the amplification values. The output from the program is shown in both Figure 55 and Figure 56.

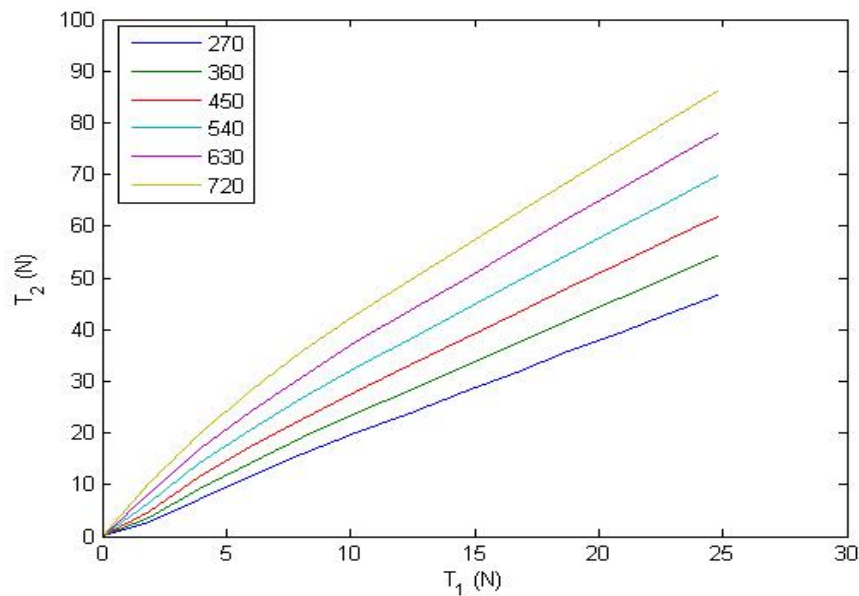


Figure 55 - Simulated experimental data comparing T2 to T1

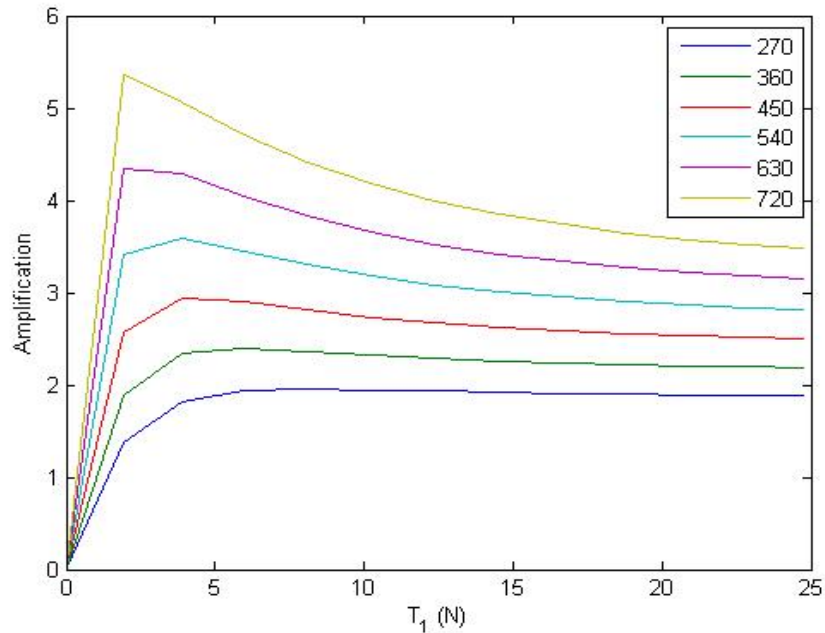


Figure 56 - Simulated amplification ( $T_2/T_1$ ) for the test data

It can be seen that the curves in Figure 55 match up exactly with the estimation curves which accurately describe the plot trends of the data. Figure 56 shows the simulated amplification values which can be compared to either of the raw data plots or the theoretical curves in Figure 47. Once the basic test setup was simulated, the next step was to explore the interaction between two control motors with the single drive capstan. This was done by taking the simulation created for the experimental replication and doubling it. The two systems are independent of each other so duplication should accurately describe the system.

The simulation was created in such a way that the user is able to easily determine the input servo angles and the simulation shows the applicable results. An example run is shown with the first control motor incrementally increasing its angle and the second

control motor increasing its angle in a step pulse manner, the plots illustrating the individual changes are shown in Figure 57 and Figure 58 respectively. Simulink does not allow for axis labeling so for reference, when viewing the Simulink plots, unless otherwise noted the x-axis is time and the y-axis is angle. The angle of contact for both the control motors is 720 degrees and the drive motor's voltage is set to 10V.

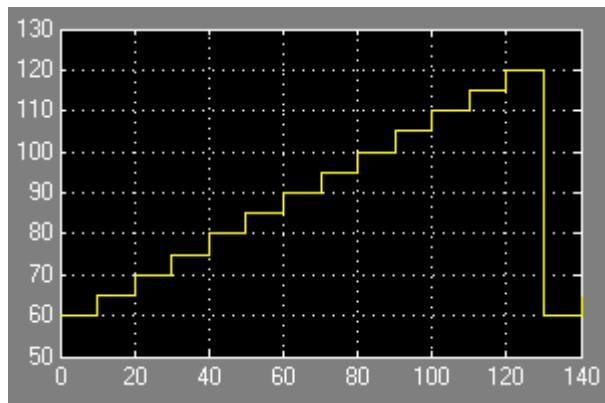


Figure 57 - Sample test input for control motor 1 in simulation

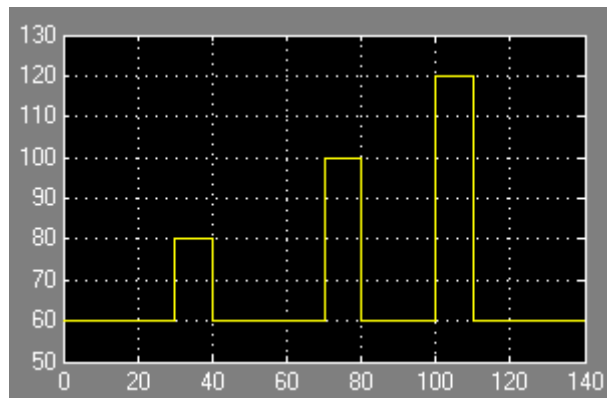


Figure 58 - Periodic stepping input provided by control motor 2 in simulation

The results from running the simulation with these parameters are shown below.

Figure 59 shows the estimated current needed to supply the two systems with the needed friction (y-axis = Current (A)) and Figure 60 solves for the power consumption of the drive motor (y-axis = Power (W)). A sign that the simulation is working properly was that the current values which were estimated by the simulation were roughly the same as the current observed in preliminary experimentation. Since friction and mechanical dynamics are not taken into consideration in this model, the result is a rough estimate.

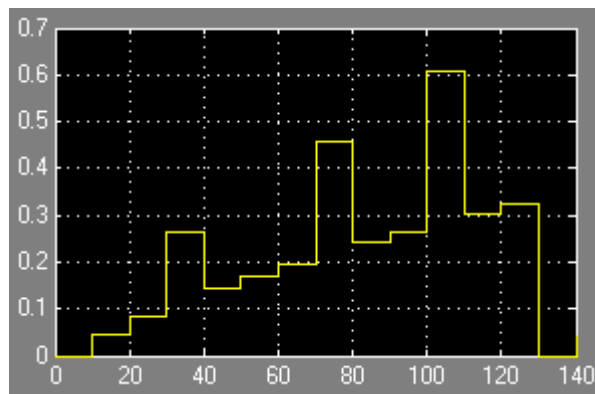


Figure 59 - Simulated estimate for the drive current needed for amplification

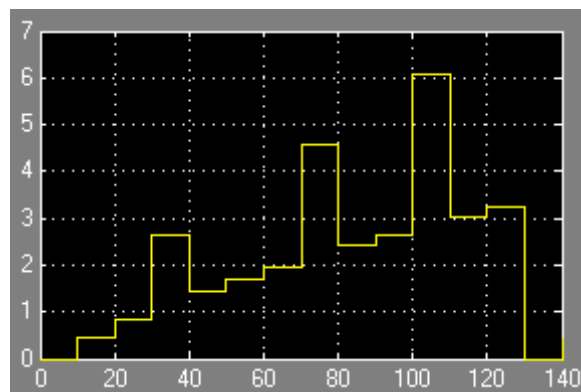


Figure 60 – Simulated estimate of drive motor power consumption

## DISCUSSION

There were numerous observations made throughout the testing and simulation process. While running the test runs, it was noticed that the capstan underwent mild warming. This effect is obvious since friction is involved but it is unclear if this would have a major effect in a system that employed numerous control motors all generating heat. Heat is not the only consideration which needs to be addressed in a system that relies on friction. It was also noticed that the capstans were undergoing a degree of polishing due to the friction. The effect of the polishing was not noticed in the data so it was not taken into consideration. In addition to the wear on the capstan, the string sections also exhibited wear. Again the effects of this wear was not noticed in the data and thus not taken into consideration. New strings for each test run downplayed this effect, but may have a noticeable effect with prolonged use.

The basic capstan equation was shown to have slight adherence to the test data but the coherence was slight. For this reason the adapted equation was derived. Basic exponentials were employed because of their ability to fit to the test data. There was no computer program which would fit the curves to the data using a conditioning equation; rather they were fit by sight with confirmation of fits given by the statistical data found from the MATLAB curve fitting toolbox. This may have produced curves with slight variation from what is actually happening but the fitted curves were robust enough to define a curve for all of the data points so the error was determined to be minimal. The tests did however confirm the fact that diameter and rotation speed did not have a factor in the test data. Material properties of both the capstan and the cord may have significant

influence on the behavior of the system and as stated in the recommendations, should be a focus of further testing.

When the simulation for the test setup was being constructed, all real values were used to make sure the simulation was as accurate as possible. The simulation turned out to produce compellingly accurate results and was able to recreate all of the data as it was observed from the testing. Since the test simulation produced accurate results it was used to develop the full system simulation. This full simulation however is not based on any test data and therefore can only be taken as an estimation of the probable behavior. There was a small level of validation in the fact that the system was built using a proven simulation and that all of the results were within reasonable ranges.

## CONCLUSIONS AND RECOMMENDATIONS

### Conclusions

This thesis provided testing and insight into the behavior of a capstan friction system. The existing equation which was thought to accurately describe the nature of capstan friction was shown to allow for only a rough estimate. To provide for a better representation of the system performance, a new equation for capstan friction was derived from curve fitting to the experimental data. The assumptions made by the original capstan equation that diameter and rotational velocity of the capstan do not play a role in the force amplification were confirmed through testing.

Although the new equation can accurately represent and estimate the behavior of a capstan system, there are still unknowns as to the underlying reason. The new equation uses two exponentials to produce the curve. An initial theory for describing the fast rising region was illustrated as possibly being associated with the cord conforming to the capstan. The reasoning behind the slow decreasing region is still unknown and a reasonable theory for the cause of the shape has not been formulated. Further testing would be required to reach a conclusion.

A simulation was constructed to mimic the experimental setup. To ensure that the simulation was able to reproduce the experimental results, all parameters from the testing setup were modeled identically. Upon running the simulation, it was shown that the simulation could reproduce the experimental data accurately. Upon determining the validity of the simulation, a simulation was formulated which simulates a system involving two control motors with a single drive capstan. No real world system was

constructed to validate the behavior of the more complex system however it was observed that the results of the simulation fell into expected ranges. The simulation results suggest the system would work as hypothesized.

Further study will be necessary to confirm the possible benefits of the hypothesized system. However, if the system was found to behave as predicted the benefits could be numerous. The system would centralize the motors, reduce volume taken up from motors, simplify the control electronics and therefore create a more efficient system. This system would be highly applicable to robots which simulate biological systems because of the specific benefits.

## Recommendations

### *Testing of Multiple Control Motors*

The end product of this system is to combine numerous control motors with a single drive capstan. It is hypothesized that the system will reduce overall weight and centralizes weight. The simulation gives insight to the possible behavior of the system but in order to validate the functionality a real world system must be built and tested. Only once the system has been built will the full benefits or drawbacks be realized.

### *Capstan and Cord Materials*

As friction is largely dependent on materials, a further study needs to be conducted where multiple materials are used for both the capstan and the cord. There might be advantages in using some materials over others and different materials may

have better wear characteristics. For any system dealing with friction there needs to be special consideration for wear and longevity.

### *Full System Integration*

If the full system tests show that the system behaves as has been hypothesized, it should be possible to integrate the new control system into an existing robot. Since the system is essentially a mechanical amplifier, the existing control scheme and structure could be kept in place. Once the system is integrated the performance can fully be tested against the previous one allowing for a direct comparison between the two.

## REFERENCES

- Attaway, Stephen W. "The Mechanics of Friction in Rope Rescue." *International Technical Rescue Symposium*. 1999.
- Bundhoo, V., and E. J. Park. "Design of an Artificial Muscle Actuated Finger towards Biomimetic Prosthetic Hands." 2005: 368-375.
- Camarillo, D. B., C. F. Milne, M. R. Zinn, and J. K. Salisbury. "Mechanics Modeling of Tendon-Driven Continuum Manipulators." *IEEE Transactions on Robotics*, 2008: 1262-1273.
- Camarillo, D. B., C. R. Carlson, and K. J. Salisbury. "Configuration Tracking for Continuum Manipulators With Coupled Tendon Drive." *IEEE Transaction on Robotics*, 2009: 798-808.
- Ghorbani, R., and Q. Wu. "Adjustable Stiffness Artificial Tendons: Conceptual Design and Energetics Study in Bipedal Walking Robots." *Mechanism and Machine Theory*, 2009: 140-161.
- Hirai, K., M. Hirose, and T. Takenaka. "The Development of Honda Humanoid Robot." *Proceedings of the IEEE International Conference on Robotics and Automation*, 1998: 1321-1326.
- Iida, F., J. Rummel, and A. Seyfarth. "Bipedal Walking and Running with Sprint-Like Biarticular Muscles." *Journal of Biomechanics*, 2008: 656-667.
- Jones, L. "Dextrous Hands: Human, Prosthetic, and Robotic." *Presence: Teleoperators & Virtual Environments* 6, no. 1 (1997).

- Jung, J. H., N. Pan, and T. J. Kang. "Capstan Equation Including Bending Rigidity and Non-Linear Friction Behavior." *Mechanism and Machine Theory*, 2008: 661-675.
- Karbasi, H., J. P. Huissoon, and A. Khajepour. "Uni-drive Modular Robots: Theory, Design, and Experiments." *Mechanism and Machine Theory*, 2004: 183-200.
- Kong, K., and D. Jeon. "Design and Control of an Exoskeleton for the Elderly and Patients." *IEEE/ASME Transactions of Mechatronics*, 2006: 428-432.
- Koo, I. M., T. H. Kang, G. L. Vo, T. D. Trong, Y. K. Song, and H. R. Choi. "Biologically Inspired Control of Quadruped Walking Robot." *International Journal of Control, Automation and Systems*, 2009: 577-584.
- Li, S., L. Liu, and X. Ming. "Design of Redundant Robot for Automated Painting of Large Complex Surface." *Intelligent Robotics and Applications; First International Conference, ICIRA*. Wuhan, China, 2008. 1086-1095.
- Lin, L. R., and H. P. Huang. "NTU Hand: A New Design of Dexterous Hands." *Transactions of the ASME*, 1998: 282-292.
- MATLAB, Curve Fitting Toolbox. "Residual Analysis (Help)." *Goodness-of-Fit Statistics*.
- Tu, C., and T. Fort. "A study of Fiber-Capstan Friction." *Tribology International*, 2004: 711-719.

## APPENDIX

Included within the appendix is a combination of code, simulation diagram and data. The Arduino code is the program which controls the servo motor and the drive motor during testing. To better illustrate the comparison between data and estimation equation, the plots with both sets are shown enlarged for detail. There are two m-files included, one is associated with the experimental simulation and the other with the two control motor with single drive simulation. Both m-files set variables for the Simulink models but each must be used with the appropriate simulation. The simulation is performed within the Simulink test environment. As stated before, the m-files associated with the Simulink models must be executed before the simulation will work. The conditioned data which was used for the data analysis is located at the end of the appendix.

## Arduino Code

The following code is the program for running the tests. When properly set up, the Arduino will incrementally increase the angle of the servo after the control button is depressed. The Arduino will also trigger the data collection and supply the control voltage to the Power Amplifier.

```
// Capstan Test Procedure
// Mike Starkey
//
// Adapted from two examples found on the Arduino Tutorial Webpage
// "Button" developed by DojoDave (2005) and
// "Sweep" developed by BARRAGAN

#include <Servo.h>

Servo myservo; // create servo object to control a servo

int pos = 0; // variable to store the servo position
int a = 0;
int buttonState = 0;

const int buttonPin = 2;
const int ledPin = 13;

void setup()
{
  myservo.attach(9); // attaches the servo on pin 9 to the servo object
  pinMode(ledPin, OUTPUT);
  pinMode(buttonPin, INPUT);
}

void loop()
{
  buttonState = digitalRead(buttonPin);
  myservo.write(125);
  if (buttonState == HIGH){
    delay(1000);
    digitalWrite(ledPin, HIGH);
  }
}
```

```
delay(500);  
digitalWrite(ledPin, LOW);  
  
for(pos = 125; pos > 60; pos -= 5)  
{  
  myservo.write(pos);  
  delay(10000);  
}  
}  
else{}  
}
```

### Comparison between Data and Estimation Equation

After all of the experimental data curves were fitted with the new equation, a full comparison between the predicted curves and the data are plotted against each other.

These plots are enlarged to show detail.

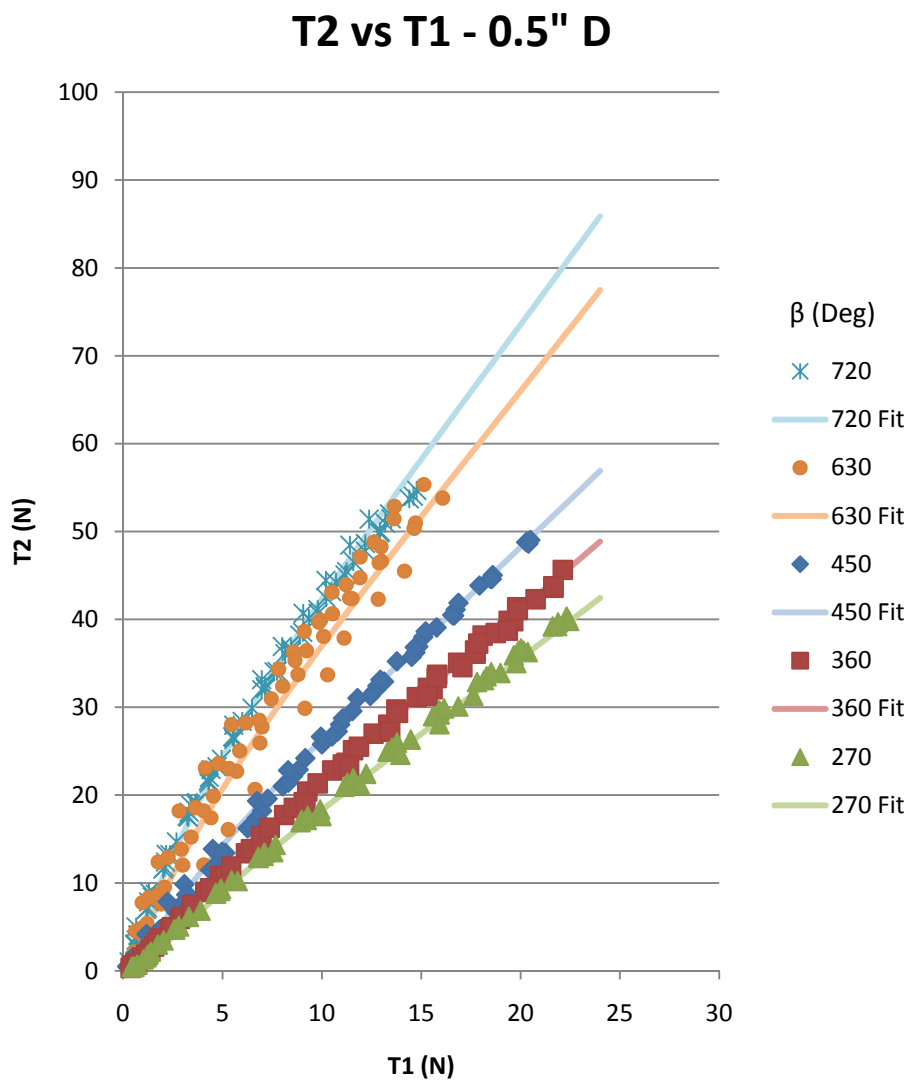


Figure 61 - Comparison between the experimental data and the double exponential estimation equation – 0.5" Diameter

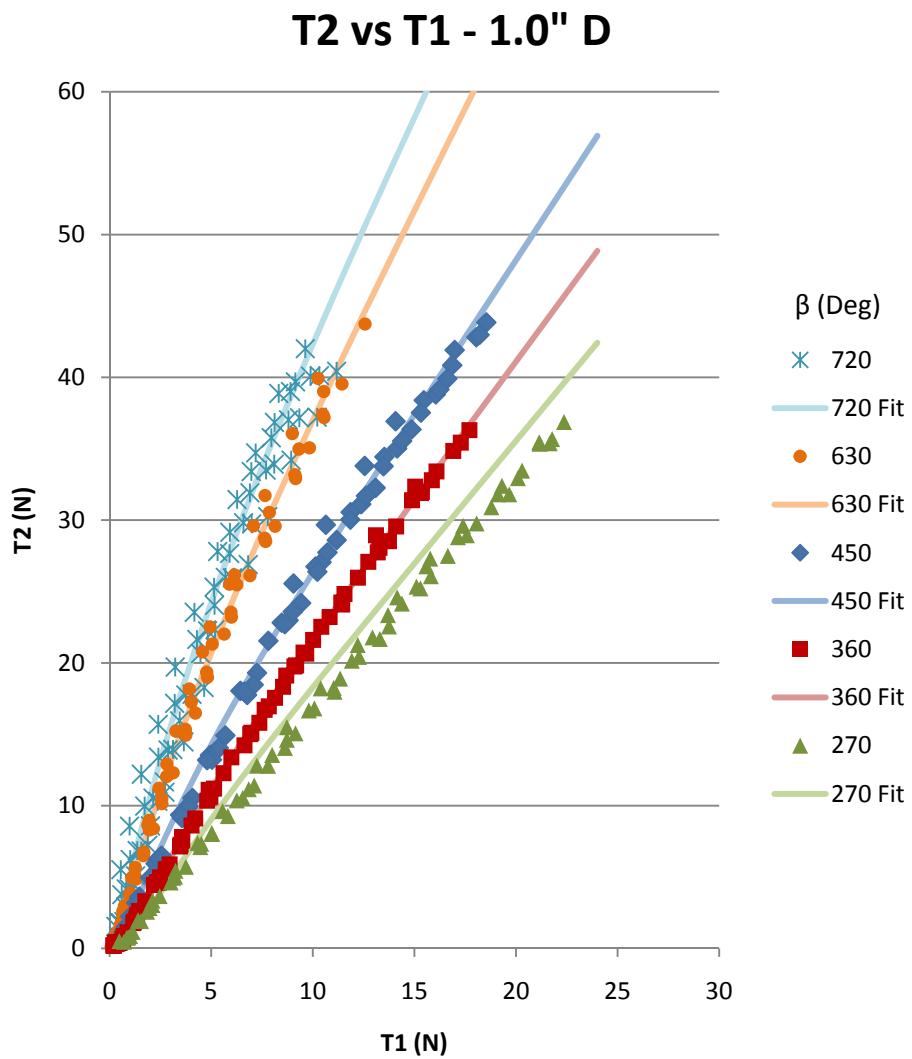


Figure 62 - Comparison between the experimental data and the double exponential estimation equation – 1.0" Diameter

## MATLAB Code

To be able to run the Simulink models, the appropriate m-file must be run. The m-files establish the simulation variables and in the case of the experimental simulation, will execute the simulation and display the results.

### *Experimental Simulation*

```

% Single Control Motor Single Drive
% Position Control
% 3/15/10
% Mike Starkey

clear;clc;

% Global Variables
DR = pi/180;
RD = 180/pi;
g = 9.81;           % m/s^2

Set = [270 360 450 540 630 720];
lamd = 0.11;

% Control Motor Variables
% -----
% HiTeck HS-322HD
% Control System: +Pulse Width Control 1500usec Neutral
% Required Pulse: 3-5 Volt Peak to Peak Square Wave
% Operating Voltage: 4.8-6.0 Volts
% Operating Temperature Range: -20 to +60 Degree C
% Operating Speed (4.8V): 0.19sec/60° at no load
% Operating Speed (6.0V): 0.15sec/60° at no load
% Stall Torque (4.8V): 42 oz/in (3.0 kg/cm)
% Stall Torque (6.0V): 51 oz/in (3.7 kg/cm)
% Current Drain (4.8V): 7.4mA/idle and 160mA no load operating
% Current Drain (6.0V): 7.7mA/idle and 180mA no load operating
% Dead Band Width: 5usec
% Operating Angle: 40 Deg. one side pulse traveling 400usec
% Direction: Clockwise/Pulse Traveling 1500 to 1900usec
% Motor Type: Cored Metal Brush
% Potentiometer Drive: 4 Slider/Direct Drive
% Bearing Type: Top/Resin Bushing
% Gear Type: Heavy Duty Resin
% 360 Modifiable: Yes
% Connector Wire Length: 11.81" (300mm)
% Dimensions: 40*20*36.5mm
% Weight: 1.51oz (43g)

```

```

Cc = 0.001;
%Jc = 0.000000043;    % kg*m^2
Jc = .00002;
Kc = 0.00055;        % Nm/A
Rc = 7.4;            % Ohms
rc = 0.00635;        % m (0.25 in)
Nc = 44;

% Drive Motor Variables
% -----
% Pittmann Gml4904S016 Lo-Cog DC Servo Gearmotor
% Assigned power rating      W      90
% Nominal voltage           V      24
% No load speed             min-1 179
% Stall torque              mNm    20.7
% Max. continuous torque    mNm    2.6
% No load current           A      0.26
% Max. efficiency           %      84
% Torque constant           mNm / A-1 6.12e-02
% Mechanical time constant  ns     7.0
% Rotor inertia             kg-m2 2.6e-05
% Motor lenght              mm     28.7
% Weight                    g      648
% Max Allowable Torque      N-m    3.53
% Reduction Ratio          N      19.7

Cd = 0.001;
Jd = 0.000026;        %kg*m^2
Kd = 0.0612;         % Nm/A
Rd = 46.5;           % Ohms
rd = 0.00635;        % m (0.25 in)
Nd = 19.7;

% Amplification Cacluation
T1m = zeros(13,6);
T2m = zeros(13,6);
Ampm = zeros(13,6);

for i=1:6
    angle = Set(i);
    G = sim('TestSimulation.mdl',[0 140]);
    T1m(:,i) = T1(1:13);
    T2m(:,i) = T2(1:13);
    Ampm(:,i) = Amp(1:13);
end

Ampm(1,:) = [0];

figure(1);
plot(T1m, T2m);
legend('270', '360', '450', '540', '630', '720');

```

```
xlabel('T_1 (N)');ylabel('T_2 (N)');  
axis([0 30 0 100]);  
  
figure(2)  
plot(T1m, Ampm);  
legend('270','360','450','540','630','720');  
xlabel('T_1 (N)');ylabel('Amplification');
```

*Two Control, Single Drive System*

```

% Double Control Motor Single Drive
% Simulation Setup
% 4/3/10
% Mike Starkey

clear;clc;

% Global Variables
DR = pi/180;
RD = 180/pi;
g = 9.81;           % m/s^2

Set = [270 360 450 540 630 720];
lamd = 0.11;

% Control Motor Variables
% -----
% HiTeck HS-322HD
% Control System: +Pulse Width Control 1500usec Neutral
% Required Pulse: 3-5 Volt Peak to Peak Square Wave
% Operating Voltage: 4.8-6.0 Volts
% Operating Temperature Range: -20 to +60 Degree C
% Operating Speed (4.8V): 0.19sec/60° at no load
% Operating Speed (6.0V): 0.15sec/60° at no load
% Stall Torque (4.8V): 42 oz/in (3.0 kg/cm)
% Stall Torque (6.0V): 51 oz/in (3.7 kg/cm)
% Current Drain (4.8V): 7.4mA/idle and 160mA no load operating
% Current Drain (6.0V): 7.7mA/idle and 180mA no load operating
% Dead Band Width: 5usec
% Operating Angle: 40 Deg. one side pulse traveling 400usec
% Direction: Clockwise/Pulse Traveling 1500 to 1900usec
% Motor Type: Cored Metal Brush
% Potentiometer Drive: 4 Slider/Direct Drive
% Bearing Type: Top/Resin Bushing
% Gear Type: Heavy Duty Resin
% 360 Modifiable: Yes
% Connector Wire Length: 11.81" (300mm)
% Dimensions: 40*20*36.5mm
% Weight: 1.51oz (43g)

Cc = 0.001;
%Jc = 0.000000043;   % kg*m^2
Jc = .00002;
Kc = 0.00055;       % Nm/A
Rc = 7.4;           % Ohms
rc = 0.00635;      % m (0.25 in)
Nc = 44;

```

```

% Drive Motor Variables
% -----
% Pittmann Gm14904S016 Lo-Cog DC Servo Gearmotor
% Assigned power rating      W      90
% Nominal voltage           V      24
% No load speed             min-1 179
% Stall torque              Nm     20.7
% Max. continuous torque    Nm     2.6
% No load current           A      0.26
% Max. efficiency           %      84
% Torque constant           mNm / A-1 6.12e-02
% Mechanical time constant  ns     7.0
% Rotor inertia             kg-m2 2.6e-05
% Motor length             mm     28.7
% Weight                   g      1268
% Max Allowable Torque      N-m    3.53
% Reduction Ratio          N      19.7

Cd = 0.001;
Jd = 0.000026;           %kg*m^2
Kd = 0.0612;           % Nm/A
Rd = 46.5;             % Ohms
rd = 0.00635;         % m (0.25 in)
Nd = 19.7;

% Amplification Cacluation

C1_angle = 720;       % Angle of contact in cord attached to C1
C2_angle = 720;       % Angle of contact in cord attached to C2

DriveV = 10;         % Drive Voltage

```

### Simulink Models

The math for the simulation is carried out within the Simulink environment. To be able to run the simulation, an initial run of the associated m-file is needed to establish necessary simulation variables. When simulating the experimental setup, the Simulink model is executed from the m-file. The theoretical system is executed separately from the Simulink environment. Subsystems associated with the larger simulation are included along with the full simulation.

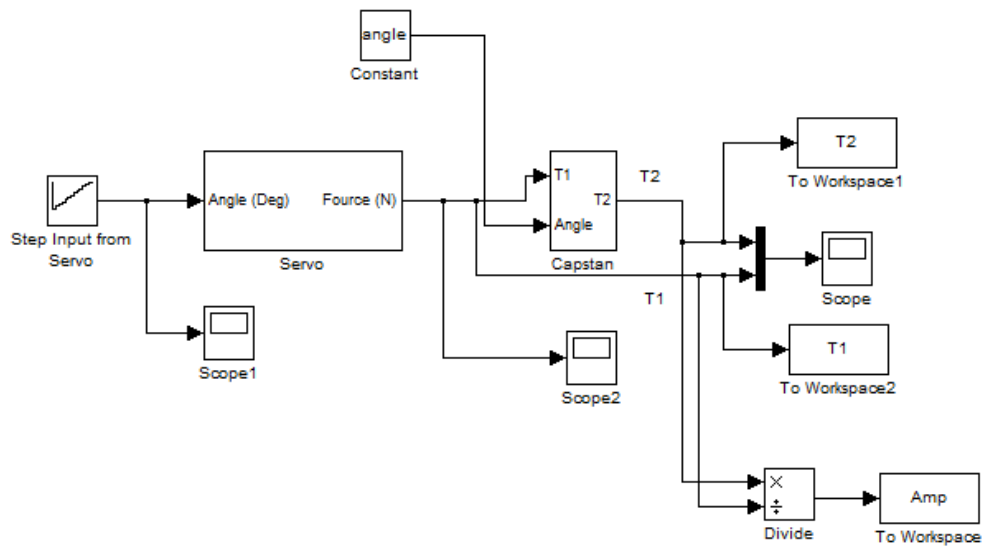


Figure 63 - Full system Simulink model

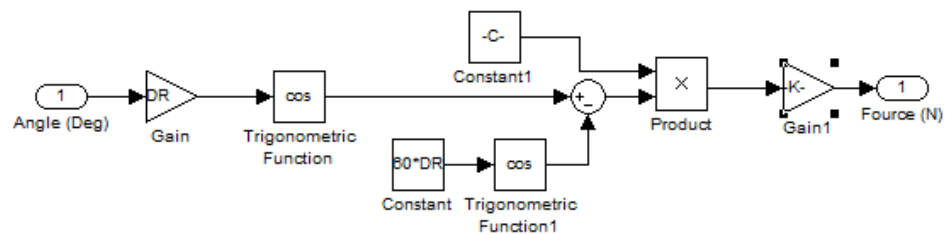


Figure 64 - Servo Simulink subsystem

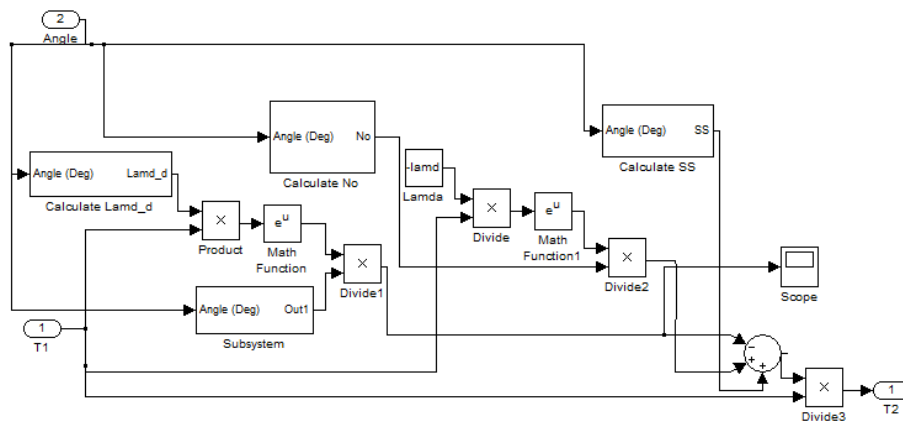


Figure 65 - Capstan Simulink subsystem

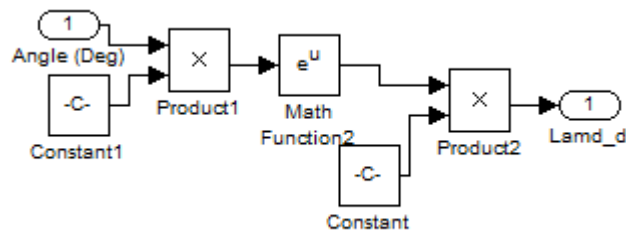


Figure 66 - Simulink subsystem to calculate Lambda d

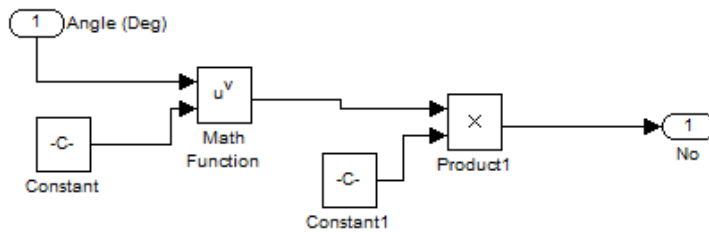


Figure 67 - Simulink subsystem to calculate No

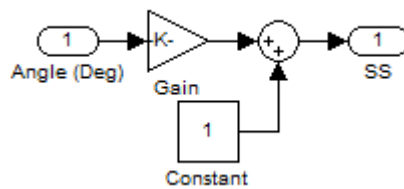


Figure 68 - Simulink subsystem to calculate steady state (SS)

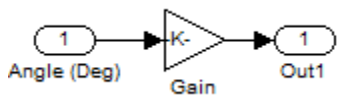


Figure 69 - Simulink subsystem to calculate Nd

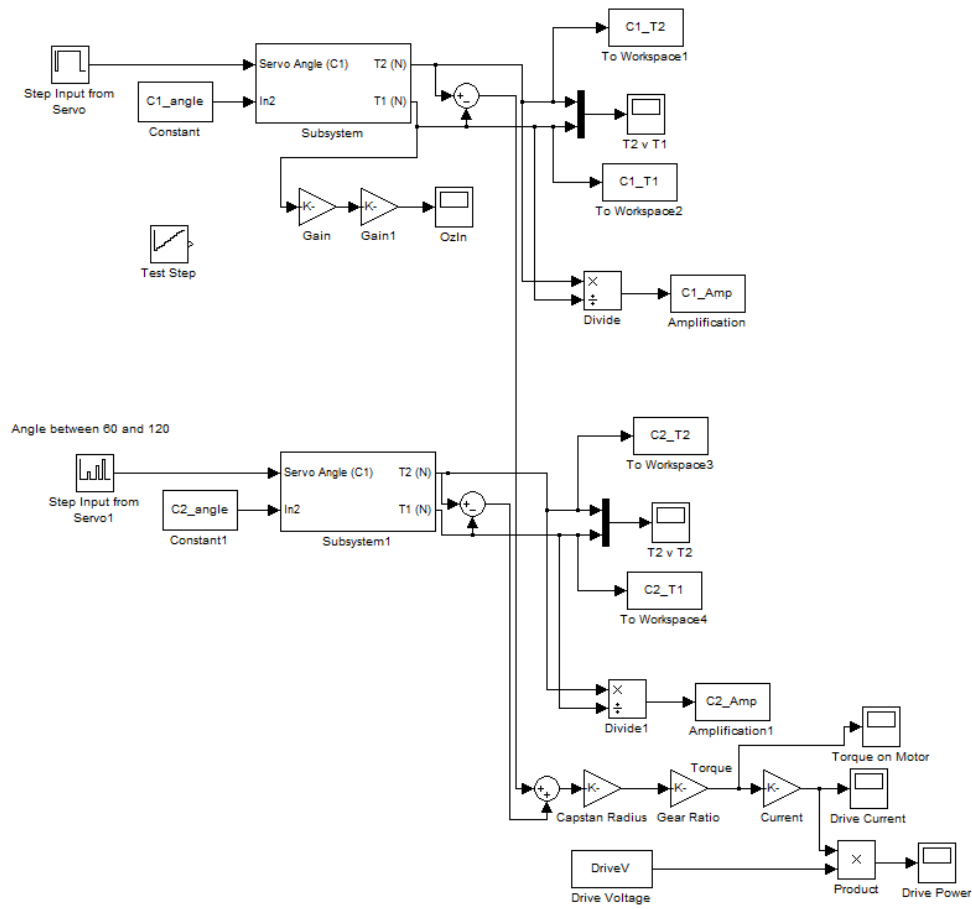


Figure 70 - Two control, single drive system simulation

### Conditioned Data

With each run of the experiment, there are over 4000 data points which are recorded. To reduce the amount of data, averaging was performed over the individual steps in the testing process. Each increase of the angle of the servo caused the two tensions to increase in a stepwise manner. A selection of 210 samples were averaged across a time period defined as two seconds after the force was increase to one second before the next force change. The numbers 1-12 for each of the data sets are step counters and serve as reference only. There are six sets of data for each counter representing the six runs for each angle. The values for the T1, T2 and Amplification are shown in each set and are associated with one another horizontally.

## 0.5 Inch capstan

## 270 Degrees

	T2	T1	Amp		T2	T1	Amp
1	0.433063	0.435185	0.995124	7	21.39158	11.27416	1.897399
	0.418189	0.446235	0.93715		17.60962	9.982716	1.764011
	0.69998	0.710065	0.985797		22.41876	12.22952	1.833167
	0.460334	0.563191	0.817367		21.22217	11.46319	1.851332
	0.425626	0.486523	0.874832		20.94451	11.13748	1.880543
	0.412569	0.497913	0.828598		21.89947	11.58338	1.890594
2	1.51918	1.157991	1.311911	8	25.39725	13.52636	1.877611
	1.293138	1.021263	1.266214		21.20346	11.90269	1.781401
	2.988162	1.742192	1.715174		26.3238	14.47131	1.819034
	2.153923	1.387637	1.552224		25.19809	13.62229	1.849769
	1.67846	1.195688	1.403761		24.95189	13.30094	1.875949
	1.8734	1.273527	1.471033		25.97763	13.78173	1.884932
3	4.696644	2.559749	1.834806	9	29.65444	15.91312	1.863521
	3.448303	2.033642	1.695629		24.59161	13.95173	1.762621
	6.138249	3.308729	1.855168		30.07919	16.86644	1.783375
	5.046959	2.803876	1.799993		29.17828	15.9291	1.83176
	4.699596	2.617036	1.79577		28.98508	15.5954	1.858566
	5.126272	2.793552	1.835037		29.87508	16.15043	1.849801
4	8.864003	4.658851	1.902616	10	33.5263	18.28691	1.83335
	6.846177	3.893879	1.75819		28.07376	15.91618	1.76385
	10.28635	5.455101	1.885638		33.89304	18.98049	1.785678
	9.078197	4.872533	1.863137		33.08585	18.15772	1.822137
	8.780209	4.67415	1.878461		32.8738	17.81008	1.845798
	9.330735	4.921491	1.895916		33.99006	18.51929	1.835386
5	12.99766	6.802642	1.910678	11	36.43626	19.88944	1.83194
	10.21148	5.76228	1.772125		31.30641	17.61948	1.776807
	14.3258	7.6674	1.868404		36.28028	20.36247	1.781723
	13.0803	7.064432	1.851571		36.44021	20.15368	1.808117
	12.83751	6.815392	1.883606		35.91687	19.65817	1.827071
	13.44555	7.104381	1.892572		36.70072	20.023	1.832929
6	17.18396	8.97562	1.914515	12	40.31508	22.31695	1.806478
	13.51647	7.553997	1.789314		35.02219	19.7832	1.7703
	18.37791	9.911704	1.854163		39.83546	22.44768	1.774591
	17.17114	9.235803	1.859193		39.25386	21.84216	1.79716
	16.92114	8.926424	1.895624		39.2094	21.61624	1.813886
	17.62561	9.282464	1.898807		39.67233	21.88721	1.812581

## 360 Degrees

	T2	T1	Amp		T2	T1	Amp
1	0.535127	0.533179	1.003655	7	25.10537	11.57053	2.169767
	0.595948	0.441552	1.349666		19.11255	9.169373	2.08439
	0.666189	0.667984	0.997314		23.67278	11.24007	2.106106
	0.551324	0.480311	1.147849		22.80922	10.52456	2.167237
	0.482736	0.460081	1.049239		23.48222	11.05086	2.124921
	0.336634	0.378314	0.889825		21.33035	9.78883	2.17905
2	2.329752	1.363687	1.708421	8	29.74387	13.74843	2.163437
	1.526814	0.982235	1.554429		23.20587	11.36837	2.041266
	2.768762	1.564398	1.769858		27.945	13.37263	2.089717
	1.835271	1.178259	1.557612		26.98918	12.60225	2.141615
	1.783168	1.159716	1.53759		28.01347	13.34943	2.098478
	0.866317	0.704907	1.22898		25.50721	11.86577	2.149646
3	5.892831	2.851447	2.066611	9	33.70042	15.8027	2.132574
	3.684273	1.847005	1.994729		27.20501	13.43571	2.024829
	6.134706	2.985048	2.055145		32.05347	15.57321	2.058245
	4.7425	2.360562	2.009056		31.1529	14.77883	2.107941
	4.962135	2.453678	2.022325		32.19677	15.33709	2.099275
	3.240672	1.700043	1.90623		29.36315	13.82992	2.123161
4	10.82209	4.87958	2.217832	10	38.15124	18.09252	2.108675
	7.111531	3.467781	2.050744		31.30825	15.32128	2.043449
	10.4651	4.976816	2.10277		36.10251	17.73927	2.035175
	8.985238	4.133817	2.173594		35.05997	16.86023	2.079448
	9.410487	4.372488	2.152204		36.45752	17.71258	2.058284
	7.489512	3.456732	2.166645		33.33352	15.78264	2.112037
5	15.34199	6.940414	2.21053	11	41.38087	19.83331	2.086433
	10.77482	5.14919	2.092528		34.56102	17.07273	2.02434
	14.63066	6.947384	2.105923		39.79737	19.62858	2.027522
	13.37705	6.181562	2.164025		38.44234	18.7515	2.050095
	13.85271	6.426183	2.155667		39.83041	19.39933	2.053184
	11.85555	5.436649	2.180671		37.24691	17.86884	2.084462
6	20.40832	9.263189	2.203164	12	45.62707	22.12341	2.062389
	14.69366	6.939631	2.117354		38.72259	19.36084	2.000047
	19.20451	9.090071	2.112691		43.60362	21.66018	2.013078
	17.73475	8.107665	2.187405		42.28854	20.75496	2.037515
	18.53817	8.585766	2.159175		43.76526	21.65219	2.021286
	16.28028	7.372762	2.208166		41.07213	19.86674	2.067381

## 450 Degrees

	T2	T1	Amp		T2	T1	Amp
1	1.021613	0.697277	1.465146	7	25.77779	10.00342	2.576898
	0.462657	0.203445	2.274114		19.33426	6.735796	2.870376
	0.568267	0.231154	2.458392		19.58928	7.270256	2.694442
	1.720886	0.932718	1.845022		28.02914	10.9207	2.566606
	1.742702	0.930848	1.872165		27.24674	10.79746	2.52344
	0.829565	0.669058	1.2399		26.68828	10.51459	2.538215
2	3.509372	1.44118	2.435069	8	29.57206	11.53448	2.563797
	1.586323	0.499163	3.177965		22.82033	8.302265	2.748687
	0.653228	0.351024	1.860918		24.20424	9.16511	2.640911
	4.782622	1.912086	2.501258		32.42833	12.79534	2.534386
	4.079927	1.662267	2.454435		31.84588	12.66536	2.514408
	3.116125	1.342149	2.321743		31.28806	12.43731	2.515663
3	6.779664	2.624222	2.583494	9	32.91761	13.13215	2.506642
	4.174148	1.169179	3.570154		26.64762	9.953948	2.677091
	1.598743	0.846105	1.889532		28.74594	11.05976	2.599147
	8.554068	3.316724	2.579071		36.91045	14.85385	2.484909
	7.726498	3.022193	2.556586		36.23928	14.71258	2.463148
	6.852089	2.707825	2.530477		35.72776	14.521	2.46042
4	11.46658	4.386992	2.613768	10	36.82418	14.67875	2.508672
	7.858653	2.24014	3.508107		31.03266	11.79481	2.631044
	4.672508	1.821446	2.565274		33.12684	12.94312	2.559418
	13.41928	5.141254	2.610119		41.11088	16.73432	2.456681
	12.59275	4.882354	2.579238		40.43211	16.65527	2.427586
	11.79332	4.581125	2.574329		40.49293	16.56433	2.444586
5	16.2258	6.262023	2.591143	11	39.07552	15.77563	2.476955
	9.855655	3.07889	3.201042		35.22049	13.77413	2.557003
	8.667006	3.171876	2.732454		37.99548	15.1048	2.515457
	18.2142	6.994186	2.604192		45.02983	18.60028	2.420922
	17.37924	6.724746	2.584371		44.59574	18.55379	2.403592
	16.5299	6.444596	2.564924		44.62187	18.48346	2.414152
6	21.00106	8.033874	2.614064	12	43.84831	17.93431	2.444941
	13.87286	4.511176	3.07522		38.63442	15.22545	2.537489
	13.56122	4.978457	2.723981		41.87825	16.87694	2.481388
	22.90886	8.827947	2.595038		48.78404	20.28481	2.404954
	22.17398	8.544434	2.595137		48.62935	20.39752	2.384082
	21.41757	8.308934	2.577655		49.02981	20.49322	2.392489

## 630 Degrees

	T2	T1	Amp		T2	T1	Amp
1	4.01125	0.865824	4.632868	7	33.53408	8.195446	4.091795
	1.502561	0.479088	3.136291		25.93331	6.852325	3.7846
	1.774436	0.564765	3.1419		28.51092	7.454783	3.824514
	2.162664	0.629363	3.436274		30.96259	7.824009	3.957381
	4.515995	1.050438	4.299156		34.3188	8.799094	3.900265
	3.908449	0.959321	4.074184		33.7258	8.577082	3.932083
2	7.759037	1.681738	4.613701	8	36.2843	9.146299	3.967102
	3.967817	0.959383	4.135801		29.87635	8.029406	3.720867
	4.894176	1.195142	4.09506		32.39557	8.645606	3.747056
	5.371026	1.301508	4.126771		35.32032	9.112898	3.87586
	8.347026	1.916886	4.354473		38.63091	10.08746	3.829596
	7.609663	1.761615	4.319708		38.06573	9.930165	3.833344
3	12.39191	2.707909	4.576191	9	39.91298	10.28773	3.879669
	7.358791	1.773912	4.148341		33.6896	9.224418	3.65222
	8.657712	2.084232	4.153909		36.43348	9.851865	3.69813
	9.526217	2.258724	4.217521		39.67615	10.5094	3.7753
	12.9103	2.99657	4.308359		43.08888	11.52069	3.740129
	12.02526	2.814183	4.273091		42.36515	11.39575	3.717627
4	18.19999	4.060007	4.482749	10	42.4139	11.11747	3.815068
	12.05892	2.922069	4.126843		37.87251	10.53337	3.595479
	13.84602	3.418281	4.050581		40.63969	11.21811	3.622688
	15.22788	3.639443	4.184123		43.93541	11.93021	3.682703
	18.57054	4.417674	4.203691		47.09065	12.9976	3.623027
	17.41494	4.134295	4.212313		46.61367	12.88098	3.618797
5	23.08879	5.285492	4.368332	11	46.44182	12.831	3.6195
	16.07424	4.049128	3.969804		42.29948	11.91859	3.549034
	18.21156	4.54024	4.011145		44.73488	12.62052	3.544613
	19.88859	4.80713	4.137311		48.8072	13.6266	3.58176
	23.59684	5.709287	4.133062		51.45004	14.70841	3.498001
	22.70353	5.455486	4.161597		50.96335	14.63994	3.481117
6	28.03436	6.636993	4.223954	12	50.36505	14.15662	3.557704
	20.64925	5.331345	3.873178		45.48981	12.97737	3.505318
	23.03238	5.863038	3.928404		48.25699	13.65123	3.534993
	25.03649	6.170219	4.057634		52.87077	15.13238	3.493883
	28.21779	6.98458	4.040012		55.34326	16.07721	3.442343
	27.75986	6.880778	4.034408		53.80886	15.89174	3.385963

## 720 Degrees

	T2	T1	Amp		T2	T1	Amp
1	3.061473	0.588811	5.199416	7	32.36449	7.149551	4.526787
	4.992173	0.649731	7.683443		33.14737	6.97129	4.75484
	3.511182	0.652899	5.377837		31.99808	6.976667	4.586442
	1.015385	0.298462	3.402063		29.88191	6.487255	4.60625
	4.025018	0.756255	5.322304		34.02913	7.594424	4.480804
	2.94793	0.593061	4.970704		32.14749	7.1691	4.484173
2	6.977932	1.165296	5.98812	8	36.67644	8.450138	4.340336
	8.969703	1.301477	6.89194		36.91173	8.008149	4.609271
	7.842878	1.287556	6.091289		36.09687	8.147221	4.430574
	4.064138	0.758576	5.357587		34.08619	7.743277	4.402037
	8.424923	1.458517	5.776362		38.21072	8.884687	4.300739
	7.162372	1.228464	5.830349		36.35298	8.459517	4.297288
3	11.59049	2.004772	5.781451	9	41.13176	9.794824	4.199337
	13.25273	2.162136	6.129462		40.68351	9.056943	4.491969
	12.38086	2.136147	5.795886		40.09566	9.35029	4.288173
	8.717515	1.613886	5.401569		38.51069	9.038351	4.260809
	13.22654	2.352339	5.62272		42.47775	10.20383	4.162923
	11.79182	2.07967	5.670046		40.71544	9.813353	4.148983
4	17.58357	3.219295	5.461933	10	45.4464	11.24504	4.041461
	18.87285	3.390371	5.566602		44.44679	10.20253	4.356448
	18.0589	3.320101	5.439262		44.22006	10.7082	4.129552
	14.68798	2.680924	5.478699		43.16512	10.48823	4.115578
	19.03071	3.62388	5.251473		46.56232	11.58316	4.01983
	17.51003	3.279982	5.338451		45.05982	11.16769	4.034837
5	21.61641	4.287195	5.042087	11	49.99573	12.93403	3.865442
	22.90404	4.427163	5.173524		48.45036	11.40867	4.246801
	22.00894	4.332754	5.079665		48.63675	12.18813	3.9905
	19.13962	3.707687	5.162147		47.77301	12.18898	3.919361
	23.22717	4.724249	4.916584		50.93968	13.19421	3.86076
	21.36553	4.323234	4.942025		49.83629	12.91289	3.859421
6	26.58054	5.563359	4.777786	12	54.01435	14.60463	3.698441
	27.95677	5.5658	5.022957		51.40944	12.38168	4.152057
	26.643	5.510951	4.834555		52.01189	13.40107	3.881174
	24.07659	4.949841	4.864114		51.44864	13.49236	3.813169
	28.38922	5.990742	4.738848		54.69478	14.77207	3.70258
	26.33284	5.572827	4.725221		53.72429	14.39537	3.732055

## 1.0 Inch capstan

## 270 Degrees

	T2	T1	Amp		T2	T1	Amp
1	0.518837	0.480346	1.080132	7	17.98264	11.07147	1.624233
	0.773028	0.850762	0.90863		12.80313	7.254428	1.764871
	2.828536	1.965581	1.439033		20.15797	11.91991	1.691118
	0.767574	0.92046	0.833903		18.25402	11.02829	1.6552
	0.872357	1.010556	0.863244		20.42076	12.27281	1.663902
2	0.467437	0.700148	0.667626	8	18.89528	11.34839	1.665019
	1.161583	1.13306	1.025173		21.67534	13.29704	1.630088
	1.987897	1.405089	1.414784		15.49727	8.724981	1.776195
	4.945474	3.12835	1.580857		23.34719	13.70279	1.703827
	2.569547	1.844615	1.392999		21.79068	12.93785	1.684258
3	3.041443	2.106864	1.443588	9	24.15857	14.38876	1.678989
	1.920144	1.54467	1.243077		22.55518	13.74672	1.640768
	3.675958	2.463242	1.492325		25.22113	15.30057	1.648378
	3.342372	2.113651	1.581326		18.21237	10.38537	1.753656
	7.334977	4.514433	1.624784		26.76429	15.59313	1.716415
4	5.030181	3.217687	1.563291	10	25.34244	15.10338	1.677932
	5.719002	3.756345	1.522491		27.49563	16.64318	1.652065
	4.622792	3.005341	1.538192		26.0718	15.80953	1.649118
	7.103504	4.46823	1.58978		28.94392	17.58631	1.645821
	5.444487	3.247504	1.676514		21.25175	12.21247	1.740169
5	10.36766	6.256734	1.65704	11	29.59708	17.39694	1.701281
	8.07961	5.021729	1.60893		28.80526	17.14586	1.680013
	9.271399	5.82121	1.592693		30.90142	18.79004	1.644564
	8.014658	5.051138	1.586703		29.77112	18.06484	1.648014
	10.5369	6.550483	1.608568		31.81361	19.66886	1.617461
6	7.390089	4.329005	1.70711	12	24.59171	14.14805	1.73817
	13.55099	8.00223	1.693402		32.4045	19.30454	1.678595
	11.15618	6.846782	1.629405		31.81246	19.10809	1.664868
	12.78776	7.806397	1.638113		33.46548	20.30081	1.64848
	11.41054	7.118603	1.602918		32.93869	20.09777	1.638923
	14.04454	8.632135	1.627007		35.38298	21.66174	1.633432
	9.622944	5.557107	1.731646		27.30903	15.78302	1.73028
	16.67357	9.805916	1.700358		35.44959	21.14139	1.676786
	14.61703	8.722582	1.675768		35.3453	21.1691	1.669665
	16.82068	10.08098	1.668556		36.87425	22.36228	1.648948
	15.06607	9.149796	1.646602		35.67981	21.78091	1.638124

## 360 Degrees

	T2	T1	Amp		T2	T1	Amp
1	0.223503	0.215005	1.039524	7	15.80021	7.367663	2.144535
	0.394726	0.257673	1.531887		14.22598	6.63482	2.14414
	0.426128	0.321251	1.326465		15.01153	6.915989	2.170554
	0.210281	0.193415	1.087197		13.37895	5.989183	2.233853
	0.206479	0.191716	1.077009		15.10706	6.973107	2.166474
2	0.312089	0.310541	1.004985	8	16.95812	7.833276	2.164882
	0.432127	0.508333	0.850087		19.74326	9.095016	2.170778
	0.638161	0.637521	1.001003		17.55406	8.141839	2.156031
	0.682934	0.671347	1.017259		18.32352	8.532949	2.147384
	0.337035	0.386276	0.872522		16.70925	7.630286	2.189859
3	0.395279	0.473285	0.835181	9	19.10546	8.691565	2.198161
	0.871336	0.699874	1.244989		20.64261	9.674524	2.133709
	1.888589	1.207032	1.564655		23.20927	10.82347	2.144347
	2.072406	1.301161	1.592736		20.72636	9.543073	2.171875
	2.32353	1.348124	1.723529		21.60562	10.01073	2.158247
4	1.129311	0.882542	1.279611	10	19.83091	9.179456	2.160357
	1.776803	1.16594	1.523923		22.53016	10.41225	2.163812
	2.620511	1.440431	1.819255		24.23148	11.39652	2.126219
	4.628872	2.324797	1.991086		27.73611	13.1976	2.101603
	4.608708	2.422544	1.902425		24.82184	11.55716	2.147746
5	4.977764	2.478642	2.008263	11	25.96586	12.21521	2.1257
	3.311475	1.752768	1.889283		24.08026	11.44972	2.10313
	4.435171	2.180643	2.033882		27.07551	12.72791	2.127256
	5.553082	2.758282	2.01324		28.52199	13.74872	2.07452
	7.557851	3.575952	2.113522		31.97917	15.36752	2.080959
6	7.259863	3.494355	2.077598	12	28.94071	13.10482	2.208401
	7.799151	3.565922	2.187134		29.55856	14.09737	2.096742
	5.891232	2.949015	1.997695		28.06299	13.27946	2.113263
	7.138717	3.460186	2.063102		31.38992	14.87944	2.109617
	8.608826	4.027115	2.137715		32.79541	15.85627	2.068293
	11.19761	5.138388	2.179207		35.42249	17.28204	2.049671
	10.34242	4.802635	2.153488		32.34658	15.04016	2.150681
	11.10524	4.867892	2.281323		33.40847	16.0846	2.077046
	9.105893	4.20653	2.164704		31.9015	15.31674	2.082786
	10.62052	4.959015	2.141659		34.84916	16.91026	2.060829
	12.27322	5.607021	2.188901		17.70515	2.050312	

## 450 Degrees

	T2	T1	Amp		T2	T1	Amp
1	0.635547	0.396165	1.604247	7	22.97988	8.804567	2.609996
	0.497874	0.379846	1.310726		17.97837	6.645986	2.705147
	1.307384	0.746352	1.751698		22.81048	8.471719	2.692544
	1.509679	0.79752	1.892966		22.71627	8.625224	2.633702
	1.097321	0.686005	1.599583		24.18754	9.426064	2.566027
	0.950723	0.637216	1.491995		23.58759	9.014509	2.616625
2	2.233173	1.010562	2.209832	8	27.04687	10.42744	2.593817
	1.280662	0.728548	1.757828		21.54195	7.811589	2.757691
	3.174589	1.310508	2.422412		26.7434	10.13176	2.639561
	3.620137	1.464963	2.471145		26.38459	10.22291	2.580926
	3.521478	1.467612	2.399461		28.6013	11.17362	2.559716
	3.184296	1.334348	2.386405		27.73362	10.71966	2.587174
3	4.951409	1.984267	2.495334	9	31.11977	12.38005	2.513704
	3.264387	1.406946	2.320194		25.55551	9.049018	2.824119
	5.935637	2.261187	2.625009		30.55404	11.85851	2.576551
	6.200341	2.400254	2.583202		30.0336	11.84814	2.53488
	6.497912	2.554908	2.543305		32.25901	13.08756	2.46486
	6.133033	2.43325	2.520511		31.6984	12.61617	2.512522
4	9.137058	3.560259	2.566402	10	35.01742	14.14764	2.475142
	6.301623	2.420111	2.603857		29.669	10.64067	2.788265
	9.599659	3.693194	2.599283		34.4264	13.52138	2.546071
	9.864096	3.838369	2.569867		33.77341	13.47889	2.505653
	10.53114	4.07789	2.582497		36.35069	14.85567	2.446924
	9.969211	3.865568	2.578977		35.54134	14.39328	2.469301
5	13.21601	5.039375	2.62255	11	38.80207	16.05027	2.417534
	9.351748	3.471182	2.69411		33.7978	12.55226	2.692567
	13.53549	4.941289	2.739262		38.391	15.46161	2.482989
	13.61994	5.095473	2.672949		37.5238	15.32027	2.449291
	14.91073	5.696401	2.61757		39.90135	16.61916	2.400925
	14.03924	5.369163	2.614791		39.14461	16.22779	2.412197
6	17.75375	6.768894	2.622844	12	42.80925	18.04679	2.372126
	13.19146	4.796812	2.750047		36.92005	14.07216	2.623623
	18.04123	6.435001	2.803609		41.91214	16.98093	2.468189
	17.96759	6.624517	2.712287		40.84282	16.85785	2.422777
	19.29912	7.252574	2.661002		43.8508	18.53892	2.365337
	18.46611	7.090445	2.604366		42.97502	18.20301	2.360874

## 630 Degrees

	T2	T1	Amp		T2	T1	Amp
1	0.899342	0.355453	2.530128	7	22.019	5.6398	3.904217
	0.102558	0.072014	1.424132		8.651006	1.875612	4.612364
	0.626971	0.207591	3.020221		18.17176	3.912695	4.644308
	0.644986	0.227512	2.834954		17.25234	4.015625	4.296304
	0.259898	0.154752	1.679453		15.34558	3.724821	4.119817
	0.1885	0.15543	1.212761		14.94116	3.751496	3.98272
2	2.202488	0.656316	3.355836	8	26.11278	6.908995	3.779534
	0.166319	0.116749	1.42459		11.21791	2.429147	4.618043
	1.102981	0.375468	2.937619		22.52608	4.938751	4.561088
	1.029284	0.384376	2.677803		21.31814	5.049054	4.222204
	0.60216	0.285201	2.111354		19.34538	4.777863	4.048961
	0.513407	0.271533	1.890774		18.9904	4.813536	3.945209
3	4.853449	1.289405	3.7641	9	29.57663	8.143478	3.631941
	0.323365	0.210905	1.533231		15.22212	3.258464	4.671564
	2.969817	0.725827	4.091632		26.16638	6.144099	4.258782
	2.608678	0.694185	3.757901		25.46909	6.257379	4.070248
	1.753555	0.557958	3.142809		23.55257	5.971022	3.94448
	1.615594	0.534075	3.025034		23.20996	5.993623	3.872442
4	8.389048	2.156913	3.889376	10	35.06488	9.831793	3.566478
	1.144938	0.373236	3.0676		20.76738	4.566383	4.547885
	5.664842	1.259594	4.497356		31.72668	7.648341	4.148177
	5.106713	1.234311	4.137298		30.53522	7.856814	3.886463
	3.878565	1.008802	3.844724		28.72729	7.626181	3.76693
	3.633298	0.978429	3.713402		28.51062	7.675423	3.714534
5	12.30025	3.127197	3.933315	11	39.53173	11.43585	3.456825
	2.604305	0.647614	4.021385		25.51875	5.896429	4.327831
	8.974612	1.955771	4.588785		36.06313	8.990411	4.011288
	8.308064	1.951664	4.256912		34.97947	9.317383	3.754216
	6.739451	1.681766	4.007366		33.18311	9.115827	3.640165
	6.49716	1.672366	3.885012		32.9175	9.148801	3.598012
6	16.489	4.218436	3.908794	12	43.73315	12.56631	3.480191
	4.946099	1.088307	4.544763		29.59895	7.080038	4.18062
	12.90205	2.816183	4.581396		39.92888	10.25278	3.894445
	12.04948	2.809534	4.288784		39.00417	10.5314	3.703609
	10.4816	2.569604	4.079073		37.4111	10.49078	3.566095
	10.13611	2.565722	3.950585		37.18104	10.55342	3.523126

## 720 Degrees

	T2	T1	Amp		T2	T1	Amp
1	2.782693	0.696778	3.993656	7	24.30149	5.84419	4.15823
	1.877986	0.431758	4.349623		23.54007	4.47302	5.26268
	0.87494	0.310553	2.817364		20.65026	4.293337	4.80984
	1.540001	0.454877	3.38553		21.64257	4.822017	4.48828
	1.838981	0.546844	3.362899		22.24548	5.186484	4.289126
	1.790225	0.547694	3.26866		22.32085	5.315849	4.198924
2	5.516524	1.217883	4.529603	8	27.80332	6.819707	4.076908
	4.422564	0.79262	5.579677		26.88844	5.161314	5.209612
	2.89613	0.59843	4.839549		24.03296	5.137949	4.67754
	3.766623	0.82074	4.589302		25.30921	5.694257	4.444691
	4.165616	0.962766	4.326717		25.99277	6.041929	4.302064
	4.181465	0.979475	4.269089		25.95581	6.27031	4.139479
3	8.563318	1.879849	4.555322	9	31.43966	7.781949	4.040075
	7.230153	1.27682	5.662627		30.24588	5.905388	5.121744
	5.086344	1.010831	5.031845		27.65902	5.916777	4.674677
	6.227032	1.356778	4.589573		29.14599	6.587233	4.424618
	6.854056	1.55293	4.413629		29.81667	6.988078	4.266791
	6.823158	1.558193	4.378892		29.73288	7.186801	4.13715
4	12.20197	2.715455	4.493527	10	34.71108	8.930597	3.88676
	10.93878	2.00896	5.444997		34.20237	6.902741	4.954897
	8.581815	1.723371	4.979668		31.91383	6.970399	4.578479
	9.971105	2.136456	4.667125		33.4041	7.695082	4.340967
	10.53684	2.368837	4.448105		33.50029	8.098137	4.136789
	10.30116	2.390936	4.308419		33.92289	8.319809	4.077364
5	15.69172	3.65229	4.296406	11	38.87582	10.21418	3.806063
	14.46754	2.693185	5.371907		37.20915	7.954528	4.677732
	11.65673	2.398586	4.859834		35.77128	8.112092	4.409625
	13.39987	2.876099	4.659045		36.84558	8.80101	4.186517
	13.89189	3.11324	4.462198		37.02457	9.339127	3.964457
	13.93453	3.225266	4.320429		37.16855	9.625853	3.861326
6	19.71178	4.64772	4.241173	12	42.00395	11.16958	3.760565
	18.27293	3.442324	5.308312		40.41732	8.899488	4.541533
	15.94518	3.199385	4.983828		39.00423	9.142579	4.266217
	17.16938	3.745955	4.583445		39.68384	9.886642	4.013884
	17.74581	4.051953	4.379569		40.07438	10.32268	3.88217
	17.80564	4.167759	4.272233		40.12132	10.61643	3.779174